DESIGN OF A COMPACT MULTI-BAND (CELLULAR 5G/GNSS/V2X) ANTENNA AND RIGOROUS ANALYSIS OF ANTENNA PERFORMANCE ON GLASS ROOFS FOR VEHICULAR PLATFORMS

by

AHMAD ABU ELHASSAN SALIH IBRAHIM

A dissertation submitted in partial fulfillment of the
requirements for the degree of

DOCTOR OF PHILOSOPHY IN ELECTRICAL AND COMPUTER ENGINEERING

2023

Oakland University
Rochester, Michigan

Doctoral Advisory Committee:

Daniel N. Aloi, Ph.D., Chair
Amanpreet Kaur, Ph.D.
Guangzhi Qu, Ph.D.
Tony Shaska, Ph.D.

To my lovely family
My Wife Lina,
My Daughter Yasmine,
My son Ali,

To my caring Parents
Prof. Abu Elhassan S. Ibrahim,
Nawal H. Ibrahim

And to my brothers and sisters

ACKNOWLEDGMENTS

I praise and thank Allah for giving me the strength and courage to complete this research.

Special thanks to my advisor Prof. Daniel N. Aloi for his guidance, support, and patience through this journey. Many thanks to my doctoral committee members, Dr. Amanpreet Kaur, Dr. Guangzhi Qu, and Dr. Tony Shaska for their valuable comments, discussions, and suggestions.

I am grateful for my wife Lina for her support and patience during this journey and grateful for my parents' encouragement and unlimited support.

This dissertation cannot be done without the help and guidance of my professors, colleagues, and friends. Thank you all for your help and support.

AHMAD ABU ELHASSAN SALIH IBRAHIM

ABSTRACT

DESIGN OF A COMPACT MULTI-BAND (CELLULAR 5G/GNSS/V2X) ANTENNA AND RIGOROUS ANALYSIS OF ANTENNA PERFORMANCE ON GLASS ROOFS FOR VEHICULAR PLATFORMS

by

AHMAD ABU ELHASSAN SALIH IBRAHIM

Adviser: Daniel N. Aloi, Ph.D.

The growing market competition between the automakers led to the implementation of more entertainment systems and extra features to satisfy the automotive customers. The entertainment systems depend on wireless services and communication which led to increasing number of antennas mounted on and inside the vehicles. This dissertation is focused on automotive antenna design and the effect of the vehicle environment on the antenna performance.

For the first part of the dissertation, a compact multi-band monopole antenna is designed for vehicular roof top shark-fin applications. The proposed multi-band antenna covers 5G sub-6GHz, GNSS and V2X frequency bands starting at 617MHz to 5925MHz. The presented antenna is a three-dimensional monopole antenna with two branches to cover the required bands with compact size to fit inside a roof top shark-fin. The antenna is simulated, optimized and then a prototype is fabricated, and its radiation characteristics are measured when mounted on one-meter ground plane and on a vehicle's roof.

For the second part of the dissertation, the analysis of a C-V2X quarter-wavelength monopole antenna performance when mounted on vehicle's glass roof is

presented. Antenna gain measurements performed on a full glass roof exhibited a performance degradation in a linear average gain of 8 dB compared to when the same antenna is mounted on a metallic ground plane. In Addition, the antenna radiation pattern on the glass roof had deep nulls. The antenna was simulated using a full-wave, three-dimensional electromagnetic field solver on the full glass sample with low emissivity (low-E) coating on the edges of the full glass roof and the simulation results showed acceptable agreement with the measurements. Simulation shows that the C-V2X antenna performance on the full glass roof can be improved by moving the low-E coating from underneath the glass to top of the glass.

TABLE OF CONTENTS

TABLE OF CONTENTS—Continued

TABLE OF CONTENTS—Continued

LIST OF TABLES

LIST OF FIGURES

LIST OF ABBREVIATIONS

4G	Fourth Generation
5G	Fifth Generation
AM	Amplitude Modulation
CAD	Computer Aided Design
C-V2X	Cellular Vehicle to Everything
DAB	Digital Audio Broadcast
DCS	Digital Communication System
E-GSM	Extended Global System for Mobile Communication
FEM	Finite Element Method
FM	Frequency Modulation
FR4	Flame Retardant 4
GHz	Giga Hertz
GLONASS	global navigation satellite system
GND	Ground Plane
GNSS	Global Navigation Satellite System
GPS	Global Positioning System
GSM	Global System for Mobile Communication
HFSS	High Frequency Structure Simulator
LAG	Linear Average Gain
LNA	Low Noise Amplifier
Low-E	Low Emissivity

LIST OF ABBREVIATIONS—Continued

LTE	Long Term Evolution
MHz	Mega Hertz
MID	Molded Interconnect Device
MIMO	Multiple-Input Multiple-Output
OEM	Original Equipment Manufacturer
PCB	Printed Circuit Board
PCS	Personal Communications Services
PIFA	Planar Inverted-F Antenna
PVB	Polyvinyl Butyral
RF	Radio Frequency
RHCP	Right Hand Circular Polarization
RP	Radiation Pattern
SADRS	Satellite Digital Audio Receiver System
SMA	Sub-Miniature version A
TM	Transverse Magnetic
UHF	Ultra High Frequency
V2X	Vehicle-to-Everything
VHF	Very High Frequency
VLP	Vertical Linear Polarization
VSWR	Voltage Standing Wave Ratio
WiFi	Wireless Fidelity

WLAN	Wireless Local Area Network

CHAPTER ONE

INTRODUCTION

When Henry Ford introduced his model T car over a decade ago, the entertainment and extra luxury features were irrelevant compared to the vehicle itself [1]. Since then, a lot of entertainment and infotainment systems and features were added to the vehicles and most of the vehicles' passengers depend on these features. Since 1920, radios were added to the vehicles for broadcasting and communications purposes, it began with the Amplitude Modulation (AM) reception on short waves followed by the introduction of Frequency Modulation (FM) on the Very High Frequency (VHF) bands. These analog radio broadcasting systems were evolved to the digital broadcasting systems such as Digital Audio Broadcasting (DAB) and the satellite broadcasting systems such as the Satellite Digital Audio Radio Service (SDARS) [2].

The revolution in the wireless communications led to huge improvements in vehicle's infotainment systems as well as the comfort and safety services. Modern navigation systems such as the Global Navigation Satellite System (GNSS) are essential for the drivers to provide them with route and traffic information. To improve safety and efficiency in vehicles and the whole transportation system, vehicle-to-everything (V2X) is introduced to control message exchange between vehicles, infrastructure, and pedestrians which is used for safety purposes. All these wireless systems need antennas to function, hence many antennas are mounted on and inside the vehicle to support all these services and systems [2].

In this chapter, we will go over an introduction to the automotive antennas discussing their types and different antenna mounting locations on the vehicle as well as the advantages and disadvantages of each antenna mounting location. The effect of the modern new all glass roof of vehicles on antennas will be discussed briefly and then the dissertation objectives and organization will be listed.

1.1 Automotive Antennas

For the vehicular entertainment and safety systems to function, many antennas are placed in vehicles to support the wireless transmission and reception of these systems [2]. The automotive antennas must receive signals from all directions around the vehicles which can be achieved by using one omni-directional antenna or use multiple antennas to obtain the omni-directional coverage around the vehicle.

1.1.1 Antenna Placement on Vehicles

The omni-directional coverage is crucial for the automotive antennas so the antenna location on the vehicle must be chosen carefully to avoid antenna signal blockage from the vehicle metallic parts. There are many locations in which the antenna can be placed on vehicles, the antenna placement choice depends on many factors such as the car aesthetics, cost of the antenna and antenna functionality [2].

Figure 1.1 shows the popular vehicle locations in which vehicle manufacturers place antennas, the most popular antenna location is the vehicle’s roof which is an ideal antenna placement to achieve omni-directional coverage without blockage from the vehicle body. For vehicles with convertible roofs, the antenna can be placed on the trunk cover where the antennas can still have omni-directional radiation pattern with minimal blockage from the car body. Antennas can be placed on the large rear spoiler for sports cars. Spoiler antenna placement provides omni-directional coverage which is compared to the roof antenna placement. Windshields, rear glass, and side windows are popular locations for premium vehicles manufacturers.

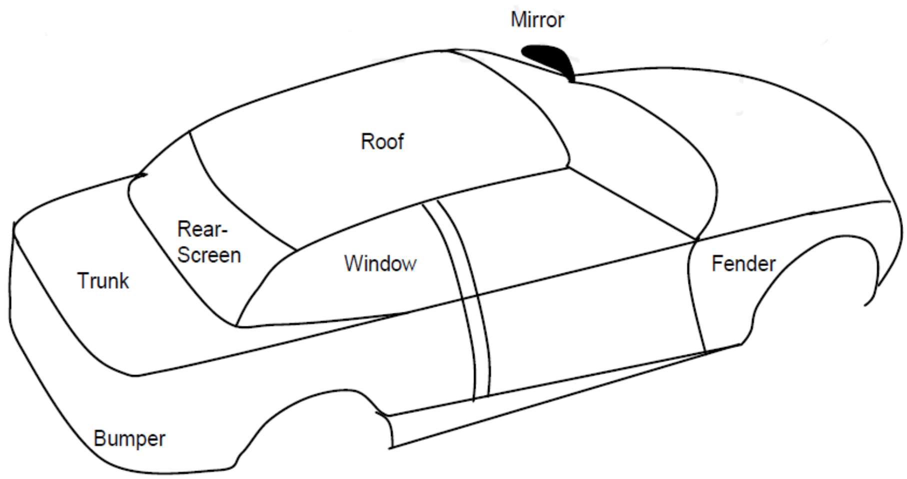

Figure 1.1 Antenna suitable locations in modern Vehicles [2].

Other less popular antenna placement in which the automotive antennas can't achieve omni-directional coverage such as fenders, bumpers, and side mirrors. To place antennas behind mirrors, fenders, and bumpers, these parts must be made of plastic to avoid antenna signal blockage. To obtain omni-directional coverage, two antennas required in the rear and front bumpers, right and left mirrors and fenders [2].

1.1.2 Automotive antenna types

Many factors are involved in the selection of the antenna type for automotive industry. One of the most important factors is the antenna size and geometry to be suitable for the vehicle placement. Antenna cost and ease of fabrication as well as the technical antenna parameters like antenna polarization and gain are also crucial in the antenna type selection [2]. Many antenna types are used in the automotive industry; the most used antenna types will be discussed briefly.

1.1.2.1 Dipole Antennas

The dipole antenna is one of the most used antenna types for low frequency applications such as the Very High Frequency (VHF), Ultra High Frequency (UHF) and lower microwave frequency bands [3]. The half wavelength dipole is the mostly used dipole antenna as its radiation resistance is 73ohms which makes it easy to be matched to transmission lines. The half wavelength dipole antenna is constructed by using two quarter wavelength rods and its feed is in the middle of the two rods as shown in Figure 1.2. The half wavelength dipole antenna has donut shape radiation pattern, so it has an omnidirectional coverage when installed vertically as the maximum gain of the donut shaped radiation pattern is perpendicular to the dipole [3].

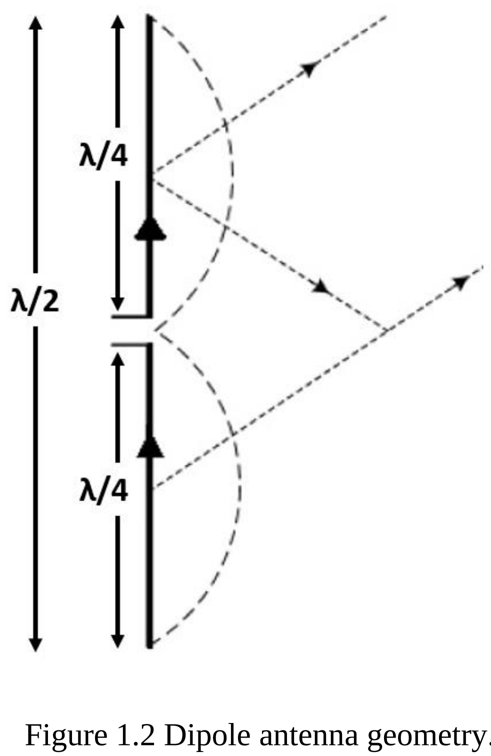

Figure 1.2 Dipole antenna geometry.

The dipole antenna is used in the automotive industry for low frequency applications with linear polarization such as AM/FM and DAB. In a few cases the crossed dipole antenna which generates circular polarization is used for satellite communication applications such as GNSS and SDARS antennas.

1.1.2.2 Monopole Antennas

A monopole antenna is a half of a dipole antenna that mounted on infinite ground plane as shown in Figure 1.3 [4]. The theory of a monopole antenna depends on the image theory which states that the fields above the ground layer can be determined through using equivalent source in free space [3], this means a monopole antenna with length L on an infinite ground plane is a dipole antenna with twice the length (2L). The monopole antenna has an input impedance equals half of the input impedance of a centered dipole antenna [4]. The monopole antenna radiation pattern is the same as the upper half of the equivalent dipole antenna, also the directivity of the monopole antenna is twice the directivity of its corresponding dipole antenna as in the monopole case there is no radiation under the ground layer. All these comparisons apply when the monopole antenna ground plane is infinite but if it is finite the image theory will not hold any more.

Monopole Antennas are the most used antenna type in the automotive industry due to their compact size and low cost. Monopoles are the perfect antennas to be placed on car roofs as the car roof will provide the monopole antenna with ground that is essential for the monopole antenna to function. Monopole antennas are widely used with application that requires vertical polarized antenna such as FM at 88 MHz to C-V2X at 5900MHz.

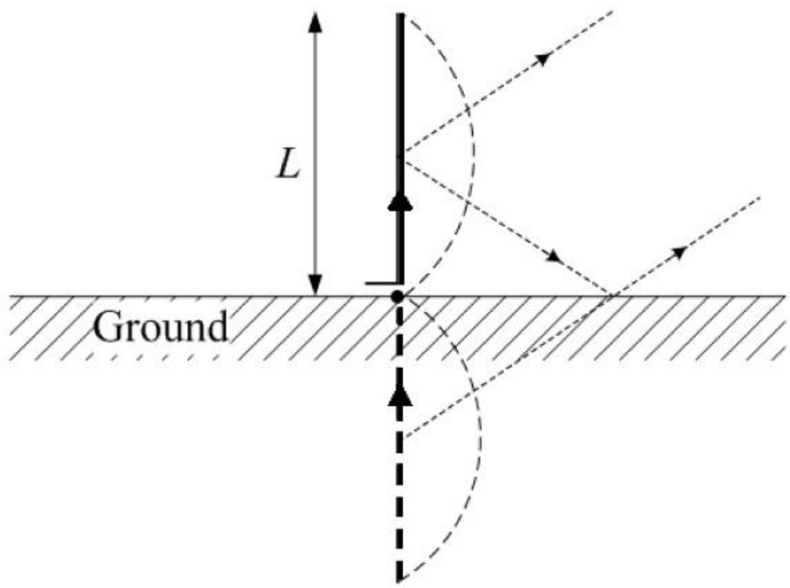

Figure 1.3 Monopole antenna geometry.

1.1.2.3 Patch Antennas

Figure 1.4 shows the conventional rectangular patch antenna geometry. It consists of a thin metallic patch usually a rectangular patch but other shapes are reported in literature such as circular, triangular, elliptical and other shapes. The metallic patch resides on a substrate with height h as shown in Figure 1.4, then there is a ground layer at the bottom of the substrate [3]. Many substrates with different dielectric constants can be used to design patch antennas. Thick substrate with low dielectric constant will result in patch antenna with wide bandwidth, high efficiency, and small losses but this comes in expense of the antenna large size which is undesirable in many applications. To get antenna with small size, thin substrate with high dielectric constant is used which will tightly couple the fields and minimize undesired radiation but in expense of narrower bandwidth and less efficiency [3].

Patch Antennas are used extensively for satellite communication in the automotive industry. Due to the patch ability to receive circular polarized waves, it is used for the Global Navigation Satellite System (GNSS) and for Satellite Digital Audio Radio Service (SDARS). Patch antennas are low profile antennas with small size which can be placed on the car roof [2].

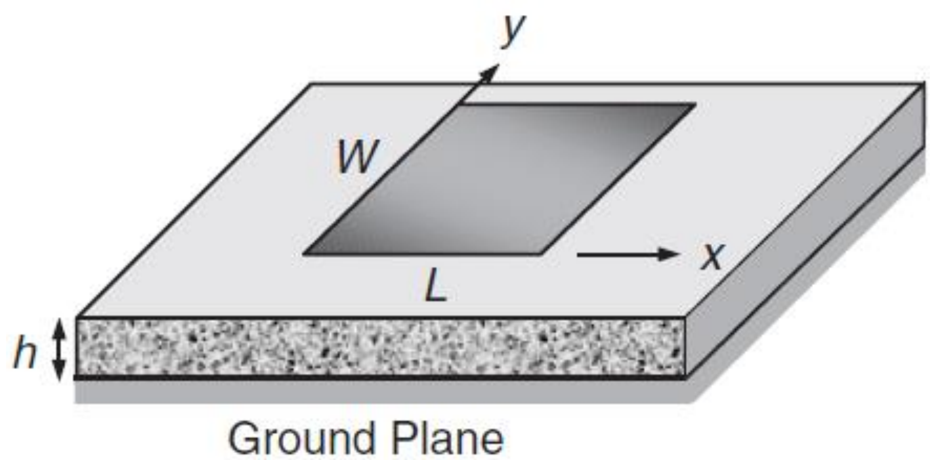

Figure 1.4 Conventional rectangular patch antenna geometry.

1.1.2.4 Planar Inverted-F antenna (PIFA)

Planar Inverted F antenna (PIFA) is widely used in the automotive industry for low profile applications. PIFA concept is derived for the microstrip patch antenna as when a short circuit plate is inserted between the patch antenna radiator and the ground plane at the position of TM_{100} mode is zero, the length of the radiator will be halved so instead of using half wavelength radiator, a quarter wavelength radiator will be enough [5]. The PIFA can also be analyzed as a wire monopole antenna above a ground plane that is folded and shorted to ground [5]. Figure 1.5 shows a planar PIFA geometry with a length L1, a width L2 and h is the PIFA height. The distance D between the shorting pin and the feed controls the impedance of the PIFA, when the feed is closer to the shorting pin then the PIFA impedance decreases and when the feed is placed farther from the shorting pin, the impedance will increase [6]. Increasing the PIFA upper plate width L2 will increase the operating bandwidth and the PIFA can be miniaturized by placing a dielectric between the top plate and the ground plane [6].

The PIFA is used extensively in the automotive industry for low profile applications for cellular, WiFi and Bluetooth communications.

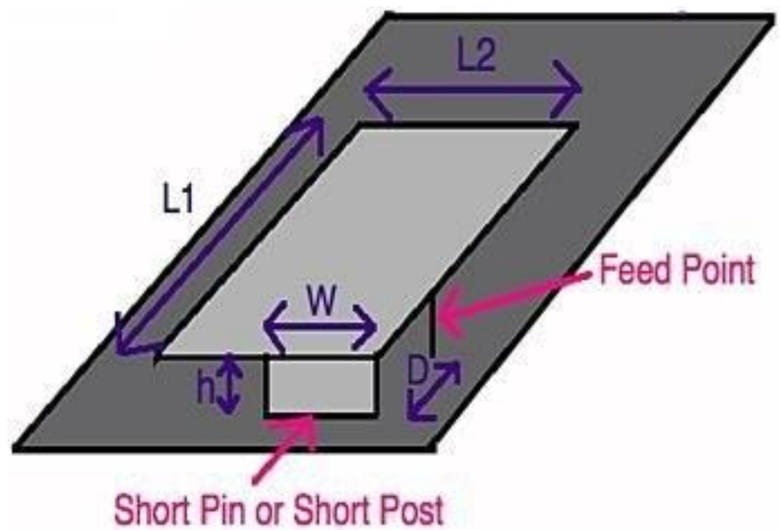

Figure 1.5 Planar inverted-F antenna (PIFA) geometry.

1.1.3 Automotive Antenna Parameters

To assess the automotive antenna performance, various parameters are used to describe the antenna impedance and radiation characteristics. In this section, the antenna parameters that will be used in the rest of the dissertation will be introduced.

1.1.3.1 Voltage Standing Wave Ratio (VSWR)

The Voltage Standing Wave Ratio (VSWR) is a parameter that describes how well the antenna impedance is matched to the antenna feed or the transmission line is connected to [7]. The VSWR is related to the reflection coefficient Γ which defines the amount of power reflected by the antenna. Equation (1.1) shows the relation between the antenna output impedance Z_0 and the antenna input impedance Z_{load} and the reflection coefficient Γ [7].

$$\Gamma = \frac{Z_{load} - Z_0}{Z_{load} + Z_0} \ (dimensionless) \tag{1.1}$$

Equation (1.2) defines the VSWR in terms of the reflection coefficient Γ [7]. Form the equation it’s clear that the VSWR will always be a real positive number that is bigger than unity, the smaller the VSWR the better the impedance matching of the antenna to its feed.

$$VSWR = \frac{1 + |\Gamma|}{1 - |\Gamma|} : 1 \tag{1.2}$$

1.1.3.2 Radiation Pattern (RP)

The antenna radiation pattern is defined as a graphical representation of the antenna radiation properties as a function of space coordinates in the far field region [3]. Radiation properties include power flux density, radiation intensity, field strength, directivity, phase or polarization. The antenna radiation pattern can be represented in two dimensions for simplicity and can also be shown in three dimensions to get the complete picture. The standard spherical coordinate system is the most used coordinate system to represent the antenna radiation properties as shown in Figure 1.6. Ɵ represents the elevation angles measured off the z-axis and Ø are the azimuth angles measured off the x-axis [3].

An isotropic antenna is a hypothetical lossless radiator having same equal radiation in all directions, although it is an ideal hypothetical antenna, but it is used as a refence to compare other antennas directive properties to it [3]. A directional antenna is defined as an antenna having the property of radiating or receiving electromagnetic waves more effectively in some directions than in others which means the directional radiation pattern has asymmetric shape. Some antennas like dipoles have omnidirectional radiation pattern which means the antenna radiation pattern is isotropic in a single plane and a directional pattern in the orthogonal plane [3].

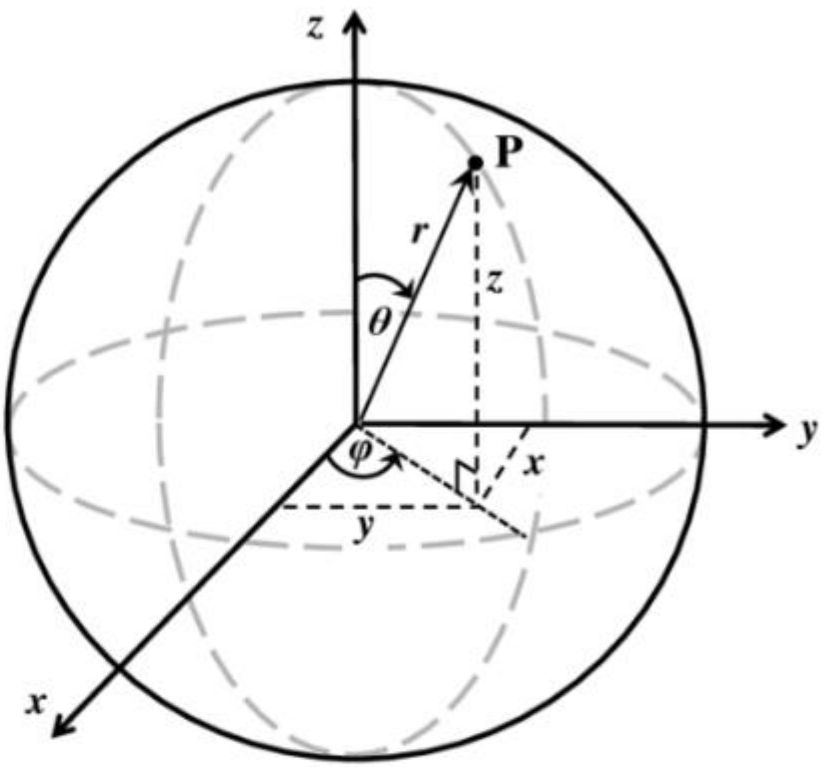

Figure 1.6 Spherical coordinate system.

1.1.3.3 Antenna Radiation Efficiency

The antenna radiation efficiency is the ratio between the power radiated by the antenna to the power delivered to the antenna input as shown in Equation (1.3) [3]. An antenna with high radiation efficiency means most of the power delivered to the antenna input is radiated by the antenna to the air which makes e_r according to Equation (1.3) be close to unity.

$$e_r = \frac{P_{radiated}}{P_{input}} \tag{1.3}$$

In practical antenna datasheets, the term antenna efficiency means the total antenna efficiency which considers the antenna losses due to the impedance mismatch at the antenna input and the losses due to the structure of the antenna such as conduction and dielectric losses [3].

1.1.3.4 Antenna Linear Average Gain (LAG)

The antenna gain is defined as the ratio of the radiation intensity in a certain direction compared to the radiation intensity if the same power accepted by the antenna is radiated isotropically [3]. The antenna gain is used to describe antennas more than the directivity as the gain takes into account the antenna efficiency and the antenna directional properties while the directivity shows only the antenna directional properties which means the directivity is only controlled by the pattern [3].

In the automotive industry, the antenna gain is expressed in linear average gain (LAG) which can be calculated using the following steps: (1) Measure the antenna gain in linear units for the required elevation angles (ϴ) at each of the 360° azimuth angles (Ø). (2) Calculate the average azimuth gain for each of the required elevation angles. (3) Calculate the average gain in linear units from the elevation angles to get one gain value for each frequency and then convert to logarithmic scale (dBi) [8].

1.1.4 Vehicle Roof-top Shark-fin

As mentioned earlier, antenna placement on vehicles has large impact on the antenna's performance so most of the antennas are placed on the vehicle's roof to avoid signal blockage by metal. Roof antennas are usually placed in one cast called a shark-fin due to its shape as shown in Figure 1.7. Shark-fins have limited size due to the vehicle's aerodynamic design; typical shark-fin has height of less than 70mm and length of less than 120mm as shown in Figure 1.7. Recently many antennas are placed inside these limited size shark-fins which increase the coupling and shadowing effects between different antennas. One solution to reduce the shadowing and coupling effects on antennas inside a shark-fin is to design antennas that cover multiple frequency bands and applications to reduce the number of antennas as well as reducing the cost [9].

(a) Side View

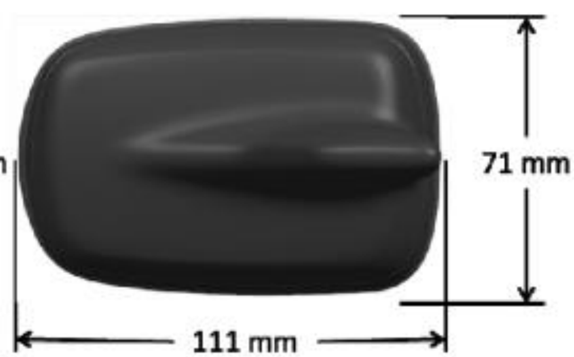

(b) Top View

Figure 1.7 Roof-top shark-fin. (a) Side View. (b) Top View [10].

1.2 Automotive Glass Roofs

The evolution of the car aesthetic designs led to the introduction of many car roof types starting with the conventional metal car roof then the sunroof and moonroof are introduced in 1970s to allow light and air inside the car as shown in Figure 1.8 (a) [11]. The revolution continued to introduce the panoramic roofs which are large glass roofs with metal parts surrounding it as shown in Figure 1.8 (b). Figure 1.8 (c) shows the new roof trend from automakers which is the full glass roof without any metal parts to present new experience and view for passengers.

There are two main glazing products for the full glass roof; tempered glass which is one piece of glass that is heated and pressured with other chemical processes to produce strong and tough glass to protect the passengers inside the vehicle. The second type of glazing is the laminated glass which consists of two layers of glass and a bonding layer between the two glass layers, the material used for the bonding layer is usually the polyvinyl butyral (PVB) [11]. The full glass roofs also contain other materials and thin films to reflect the radiation from the sun and for soundproofing purposes.

As discussed earlier, the vehicle's roof is the best location to mount the automotive antennas on and the benefit of the metallic roof is discussed in Section 1.1.1. The introduction of the full glass automotive roofs with its added materials must be studied and investigated for its effects on the roof-top antenna performance specially for the high frequency bands antennas such as V2X antennas [11].

(a) Sunroof

(b) Panoramic Roof

(c) Glass Roof

Figure 1.8 Vehicle roof types. (a) Sunroof. (b) Panoramic Roof. (c) Glass Roof.

1.3 Dissertation Contributions

In this dissertation, important automotive antenna topics are discussed including automotive antenna design and the effect of vehicle’s aesthetic design on the antenna performance. The dissertation contributions can be listed as follows:

Design of a compact multi-band antenna suitable for automotive roof-top shark-fin placement. The antenna covers the following frequency bands: 5G Sub-6GHz (617-5000 MHz), GNSS L1, E1 and B1 (1559-1606 MHz) and C-V2X (5.85-5.925 GHz). The proposed antenna is a three-dimensional monopole antenna with two branches to cover the required frequency bands with compact size (Height x Length x Width) of $58x37x17mm^3$ which fits inside a roof top shark-fin. The antenna is fabricated using a metal sheet and it is soldered on FR4 PCB which makes it a low-cost antenna and can be easily fabricated. The antenna is fabricated and measured; the measurements show the proposed antenna met the performance requirements.

The effect of the vehicle’s glass roof on the C-V2X antenna is investigated. The measurements show that when C-V2X monopole antenna is mounted on a vehicle glass roof, its performance is significantly degraded compared to the same antenna when mounted on vehicle's metallic roof. Due to a lack of information about the electrical material properties and architecture of the full glass roof sample from the glass supplier for proprietary reasons, a series of gain measurements were performed for the C-V2X monopole antenna when mounted on different glass materials. The measurements findings prove there is metal inside the glass roof sample. An assumption was made that the existence of a low emissivity layer underneath the glass at the edges of the glass roof. The simulation of the C-V2X monopole antenna when mounted on glass roof with the assumption of the low E coating underneath the glass layer shows acceptable agreement with the measurements. From the simulation results, the main reason for the C-V2X antenna performance degradation on the glass roof sample is that the C-V2X electromagnetic wave propagates through layers with different dielectric constants, which causes the wave to be reflected and scattered. Antenna simulation shows that the C-V2X antenna performance can be improved significantly when the low-E coating is installed on the upper side of the glass to be between the antenna and the glass layer.

1.4 Dissertation Organization

The rest of the dissertation is organized as follows: Chapter 2 presents a literature survey about automotive multi-band antennas and the automotive C-V2X antenna performance on panoramic glass roof. Chapter 3 discusses the proposed multi-band folded monopole antenna design and presents the antenna performance through series of simulations and measurements. The investigation of the C-V2X antenna performance on vehicle's full glass roof is presented in chapter 4. Finally, chapter 5 concludes this dissertation and explores future work ideas.

CHAPTER TWO

LITERATURE REVIEW

A literature survey is done for two different topics. The first section discusses antenna designs that can cover multiple frequency bands, and the second section is about RF material characterization for automotive glass roofs which degrades the performance of the C-V2X antenna mounted on the vehicle's roof.

2.1 Automotive Antennas with Multiple Frequency Bands

Antennas that cover multiple frequency bands are attractive in the automotive industry due to the size limitations inside vehicle's roof top shark-fin. In this section, the automotive antennas in literature are divided into three categories, multi-band antennas, wide-band antennas and the third category is antennas that combine vertical polarization with circular polarization.

2.1.1 Multi-Band Antennas

Automotive multi-band antennas are discussed in this section. Most of the multi-band antennas reported are cellular antennas that cover LTE and 5G sub-6GHz applications. Different antenna types are found in literature but the most dominant two types are monopole antennas and planar inverted F antennas (PIFAs). First the LTE antennas are discussed then followed by the 5G sub-6GHz and finally the antennas that covers other frequency bands are investigated.

In [12], Two planar monopole antennas are proposed for vehicular roof top shark-Fin. The two antennas are placed orthogonally to each other to perform in MIMO system for automotive LTE applications. The two antennas are designed on FR4 substrate with

1.6mm thickness and a dielectric constant of 4.4. The two antennas have acceptable resonance of -6dB in the LTE frequency band (698 – 2690MHz). The two antennas have maximum vertical polarized gain at elevation angle 30° of up to 7 dBi. The two antennas have almost similar size of around 65x52x1.6mm^3.

In [13] two multi-band cell antenna designs are proposed for vehicle's dashboard applications. The two antennas are designed to cover four cellular bands (GSM, E-GSM, DCS and PCS), these four frequency bands can be represented by these two bands (824-960MHz and 1710-1990MHz). The first antenna is a planar antenna that etched on an FR4 PCB while the second antenna is a 3-dimensional antenna. The planar antenna size is 24x36.5mm^2 with PCB size of 96x106mm^2 and the 3D antenna size is 30x40x14.9mm^3. The two antennas have radiation efficiency of more than 40% across the whole frequency band.

In [14] an integrated automotive shark-fin module is represented with two 4G LTE cellular antennas, GPS antenna and AM/FM antenna. The main 4G LTE antenna is printed on FR4 substrate with dielectric constant of 4.4 and thickness of 2mm and it consists of three parts to resonate at two wide band (698-960MHz and 1710-2690MHz). The antenna size is 55x25x2 mm^3. The antenna radiation efficiency is more than 30% with gain of more than -0.7dBi across the whole frequency band.

In [15] a low profile planar inverted-F antenna PIFA is proposed for automotive 4G LTE communication. The PIFA has two main parts, long branch which is responsible for the resonance in the lower frequency band (790-960 MHz) and a shorter branch which is responsible for the resonance in the lower frequency band (1710-2690 MHz) with compact antenna size of 50x50x30 mm^3. A PIFA prototype is fabricated, but no far field measurements are represented in the paper.

Ref [16] proposed an integrated LTE antenna to shark-fin for automotive roof-top applications. The antenna is integrated to the shark-fin using molded interconnect device (MID) technology. The integrated antenna resonates at two frequency bands, the first band is 791-862MHz and the second band is 1710-2690MHz. The antenna has omnidirectional radiation pattern with maximum gain of around 3 dB.

A shark-fin multi-branch LTE antenna is designed for automotive communications in [17]. The antenna size is 55x30x10mm^3. The antenna has two branches, the T-shaped branch is responsible of the lower frequency band resonance at 698-960MHz, and the conical lower part is responsible for the higher band resonance at 1427-2700MHz. The proposed antenna has good omnidirectional coverage with maximum gain of 5.2 dBi at elevation 25°.

In [18] a 3D Nefer antenna is proposed for automotive shark-fin LTE communications. The proposed antenna has similar concept to the antenna in Reference [17] as it consists of two main parts, the upper ridge part is responsible of the antenna resonance at 698-960MHz while the conical lower part is responsible for the higher frequency band resonance at 1470-2700MHz. The proposed antenna has an omnidirectional coverage with 1.5 dB deviation in its radiation pattern.

In [19] a multi-wideband branched monopole antenna is proposed for vehicular sub-6GHz 5G communications. The proposed monopole antenna has two branches, the long branch is designed to cover the lower frequency band (617-960MHz) while the higher frequency band (1710-5000MHz) is covered by the shorter branch. The antenna size (Height x Length x Width) is 60x39.8x15mm^3. The antenna has measured linear average gain (LAG) above -3 dB and radiation efficiency of more than 50% across the whole frequency band.

In [20] a dual-wideband monopole antenna is presented for automotive 5G sub-6GHz wireless communications. The proposed 3-dimensional antenna has two arms which is responsible of the dual-wideband antenna resonance. The low frequency band (617-960MHz) is produced by the long arm while the short arm is responsible of the high frequency band (1710-5000MHz) resonance. The antenna size (Height x Length x Width) is 60x36x15mm^3. The antenna has measured linear average gain (LAG) above -2 dB and radiation efficiency of more than 45% across the whole frequency band.

A multi-band inkjet-printed folded antenna is proposed in [21] for automotive LTE communications. The antenna originally is a planar wide band monopole antenna then folded around a plastic cylinder using low-cost additive manufacturing techniques. The antenna covers two main frequency bands, lower frequency band with range of 700-960MHz and higher frequency band from 1710-6000MHz which doesn't cover the lower frequency band of the 5G sub6 GHz at 617MHz. The unfolded antenna size is 84x68x0.17mm^3 with average gain above 3.9dBi.

In [22], a cellular semi T-shaped monopole antenna is presented for shark-fin roof-top automotive applications. The proposed antenna consists of a T-shaped and a cone shaped parts which are halved to miniaturize the antenna. The antenna resonates at two frequency bands, a lower band from 770 to 1000MHz and a higher band from 1700 to 3780MHz. The antenna is built on FR4 substrate with dielectric constant of 4.4 with size of 70x30x1.6mm^3. The antenna has a maximum gain of above 1.5 dBi.

In [23] a multi-band low profile Planar Inverted-F Antenna (PIFA) is proposed for the automotive 5G Sub-6GHz and Vehicle to Everything (V2X) applications. The proposed PIFA has two slots to create two frequency bands, the lower frequency band from 617 to 960MHz and the higher frequency band is from 1710 to 6000MHz. The antenna has a size of 55x50x28mm^3 with Linear average gain (LAG) of above -2.5 dBi and radiation efficiency of more than 45%.

2.1.2 Wide-Band Antennas

In this section, wide frequency band antennas for automotive applications will be discussed. There are a few wide-band antennas suitable for vehicle's roof top shark-fin reported in literature.

A wide-band Vivaldi antenna with pattern diversity is proposed for base stations LTE applications [24]. The proposed antenna is consisted of two Vivaldi slots that are rotated with an angle of 29°. The proposed antenna covers the LTE frequencies from 700 to 2700MHz with size of 260x254x0.5mm^3. The antenna has gain above 1 dBi and radiation efficiency above -1.8 dB across the whole covered frequency band.

In [25] a printed compact wide-band antenna is proposed for automotive LTE applications. The proposed antenna has a physical size of 76x25x1.53mm^3 to cover the LTE frequency band (698-2690MHz). The antenna is fabricated on FR-4 material and had a maximum gain above 2 dB with good omnidirectional coverage.

In [26] a novel miniaturized wide-band Vivaldi inspired monopole antenna is proposed for vehicular LTE applications. The proposed antenna is a monopole antenna with the shape of half Vivaldi antenna with capacitive feeding for impedance matching purposes. The antenna is built on an FR4 substrate with size of $73x69x0.81mm^3$. The antenna covers the frequency range from 620 to 4000MHz with maximum gain above 3.6dB and radiation efficiency above 80%.

In [27] a novel wide-band flat Nefer antenna is proposed for automotive flat mounting applications. The antenna has a capacitive arm for matching, and it consists of FR4 material as well as metal. The antenna covers wide frequency range from 698 to 6000MHz which covers the automotive 5G Sub-6GHz, V2X as well as WLAN applications. The size of the antenna is $80x60x30mm^3$ with measured gain above -3dBi and measured radiation efficiency above -2dB.

2.1.3 Automotive Navigation and Cellular Antennas

This section discusses the automotive navigation antennas integration with the cellular antennas. Usually, vehicles have separate antennas for cellular coverage and navigation due to the polarization difference between these two applications. A few antennas are reported in literature to integrate both GNSS and cellular antennas in one single antenna element.

In [28] a three dimensional antenna solution that fits into a top roof automotive shark-fin is proposed. The proposed antenna solution consists of GPS patch antenna which is separate from the 4G LTE antenna and WLAN antenna. Using separate antenna elements for navigation and cellular is the conventional way in the automotive industry but it is not efficient in cost wise and space wise.

An integrated GPS and cellular antenna is represented in [29]. The proposed integrated antenna consists of a dual-band PIFA for cellular coverage and a conventional patch antenna for GPS, both antennas are fabricated on FR4 substrate with size of $80x80x1.6mm^3$. The cellular dual band PIFA resonates at two narrow bands, GSM 1800 (1710–1880 MHz) and the 4G 2600 (2500–2690 MHz) while the GPS patch antenna resonates at 1575MHz. The patch antenna has a simulated RHCP gain of less than 0 dB at zenith with omnidirectional coverage.

In [30] a low profile multi-band integrated slots monopole antenna with multi-polarization property is proposed. The proposed antenna covers GPS 1575MHz with RHCP and Cellular bands (GSM850/GSM900/DCS/PCS) with linear vertical polarization using two separate feeds for GPS and cellular. The antenna is fabricated on FR4 with $70x70x0.8mm^3$ size. The antenna has a maximum gain of more than 1.8 dBc in the GPS band with more than 90% efficiency while the cellular efficiency is more than 55% with maximum gain of more than -1.55 dBi.

A novel multi-band quasi-yagi antenna is proposed for cellular, GPS and Bluetooth/WLAN applications [31]. The antenna consists of a driver dipole element, a parasitic director element, a derived driver element, and a truncated ground plane as the reflector element of the proposed antenna. The antenna is fabricated on FR4 substrate with size of $130x95x1\ mm^3$. The antenna has a maximum gain in the range of 0.3-4.4 dBi across the operating frequency band.

In [32] stacked compact tri-band antenna is proposed to cover GPS and GSM 900/1800. The proposed stacked antenna consists of two stacked elements, the truncated patch antenna is responsible of the resonance at the GPS L1 band while the upper small loops element is responsible of the GSM coverage. The GPS patch is built on F4B substrate, and the GSM loops element is built on FR4 substrate with stacked antenna dimensions of 60x60x12mm^3. The antenna has a narrow cellular band.

To summarize this section, a literature survey is conducted to investigate the multi-band antennas which are suitable for the automotive industry. Most of the automotive multi-band antennas found in literature are for LTE cellular frequency band and a few antennas cover the 5G sub-6GHz band. Wide-band antennas found in literature are not suitable for roof-top shark-fin placement due to their size and structure. The last observation in this literature survey is there is no automotive antenna that covers GNSS and 5G sub-6GHz frequencies as most of the references use separate antennas for both frequency bands.

From this literature review, multi-band antennas with compact size that covers multiple applications are required for automotive roof-top shark-fin applications.

2.2 Automotive C-V2X Antennas on Glass Roof

In this section, the problem of the performance degradation when mounting C-V2X antennas on vehicle’s Full glass roof will be addressed. Currently, there are no studies on antenna performance when mounted on a vehicle's full glass roof in any frequency band. Few references discuss the C-V2X antenna performance when mounted on metal behind a panoramic roof [33-36].

An investigation on V2X quarter wavelength monopole antenna placement on vehicle’s panoramic roof is held in [33]. The measurements setup shows that the antenna is placed on metal roof top with the panoramic glass is in front of the antenna with 250mm distance from the V2X antenna. The radiation pattern of the V2X monopole antenna at horizon shows that the metallic roof without glass has omnidirectional coverage while the radiation pattern with panoramic glass roof has omnidirectional coverage except for the glass direction which has deep nulls and that shows the effect of the glass on the V2X antenna coverage. The authors of ref [33] suggests to cover the glass with ohmic sheet which reduced the deep nulls in the glass direction [34].

A C-V2X real road measurements are conducted when the C-V2X antenna is mounted a car roof inside a shark-fin [35]. The goal of the study is to investigate the effect of the vehicle environment and characteristics on the C-V2X antenna performance by measuring the packet error rate. The measurements showed that the C-V2X antenna performance is not symmetric in all directions around the vehicle due to the antenna placement in the rear of the vehicle as the communication to the front direction of the vehicle is worse than other directions. The measurements also showed that if the antenna is placed behind a panoramic roof, the communication in the direction of the panoramic roof (front direction) is degraded significantly.

Three different Car2Car antenna types are measured on different roof configurations to see the effect of the car roof on Car2Car different antennas [36]. The three Car2Car antennas used in this study are the flush disc antenna, the flat monopole and the colinear antenna. When the three antennas were measured on a vehicle with a metallic roof, the three antennas showed similar radiation pattern that is almost omnidirectional radiation pattern at horizon but when the three antennas were measured on a panoramic glass roof, the three antennas showed a degradation in the antenna gain in the panoramic glass direction by 15 to 20 dBi. To proof that this effect is caused by the panoramic glass, the window was removed, and the horizontal diagram was very similar to the full metal roof without deep nulls. This study proves that changing the antenna type will not solve the Car2Car antenna performance degradation caused by the glass.

To conclude, the problem of mounting C-V2X antennas on vehicle's all glass roof and the corresponding degraded antenna performance was discussed. No refences found in literature investigated the effect of vehicle's all glass roof on C-V2X antennas which indicates this is new and open area for research.

CHAPTER THREE

MULTI-BAND FOLDED MONOPOLE ANTENNA

3.1 Introduction

Antennas that cover multiple frequency are attractive in the automotive industry due to the space saved in the roof-top shark-fin which has small size because of the aesthetic design of vehicles. The literature survey presented in Chapter Two shows that there are few automotive multi-band antennas due to the challenges of the compact size nature of the automotive antennas as well as the strict requirements of the automakers. In this chapter, the design of a compact multi-band monopole antenna for the automotive industry that covers 5G sub-6GHz and LTE cellular frequencies, V2X and GNSS frequency bands will be discussed.

Table 3.1 shows some general performance requirements that the proposed antenna must meet for 5G, LTE, GNSS and V2X. The performance requirements are in terms of frequency bands with its corresponding voltage standing wave ratio (VSWR) and the required linear average gain (LAG) in certain elevation angles as well as the polarization. The antenna performance requirements shown in Table 3.1 are derived from the automotive original equipment manufacturers (OEMs) specifications at the pigtail level.

Table 3.1 Antenna Performance Requirements

Application	Frequency (MHz)	VSWR	LAG	Polarization
5G Sub-6GHz & LTE	617-960 1710-2690 3300-5000	3.3 2.7 2.7	-4 dBi in elevation angles (75° - 87°)	Vertical linear Polarization
V2X	5850-5925	2	-2 dBi in elevation angles (80° - 96°)	Vertical linear Polarization
GNSS	1559-1606	2	Active LAG of 20 dBc in elevation angles (0° – 50°)	Right Hand Circular Polarization

3.2 Antenna Design and Theory

The proposed monopole antenna geometry is shown in Figure 3.1, and Table 3.2 shows the detailed dimensions of the antenna. The proposed antenna is a folded three-dimensional monopole antenna with one main slot to divide the antenna into two parts, these two parts will be called long branch and short branch in the rest of the chapter for illustration purposes as shown in Figure 3.1. The long branch is designed to cover the lower band from 617 to 960MHz, this branch is miniaturized by folding the antenna in a horizontal and vertical directions with the slot goes through the two folded parts to lengthen the current path for the antenna to be a quarter wavelength long at 788MHz which is the center frequency of the low band. The long branch folded arm is added to the antenna to reduce the antenna height to fit inside a shark-fin which has limited height, the effect of the folded arm will be studied more with the antenna current distribution and parametric sweeps for the folded arm width (W) and height (H4).

The short branch is responsible for the higher band resonance, which is from 1559 to 5925MHz to cover GNSS, high cellular and V2X frequency bands. The short branch has a horizontal top loading portion with width W2, this horizontal portion is to make a gap between the short branch and the folded arm of the long branch, this gap is important for the GNSS signal to not get blocked by the long branch folded arm which is also tapered and chamfered for the same purpose. The gap between the short and long branch is optimized to be as large as possible within the antenna dimensions. The proposed antenna is mounted on an FR4 PCB and connected to a short cable with SMA connector as a feed. The monopole antenna has a compact size (H x L x W) of 58x37x17 mm^3.

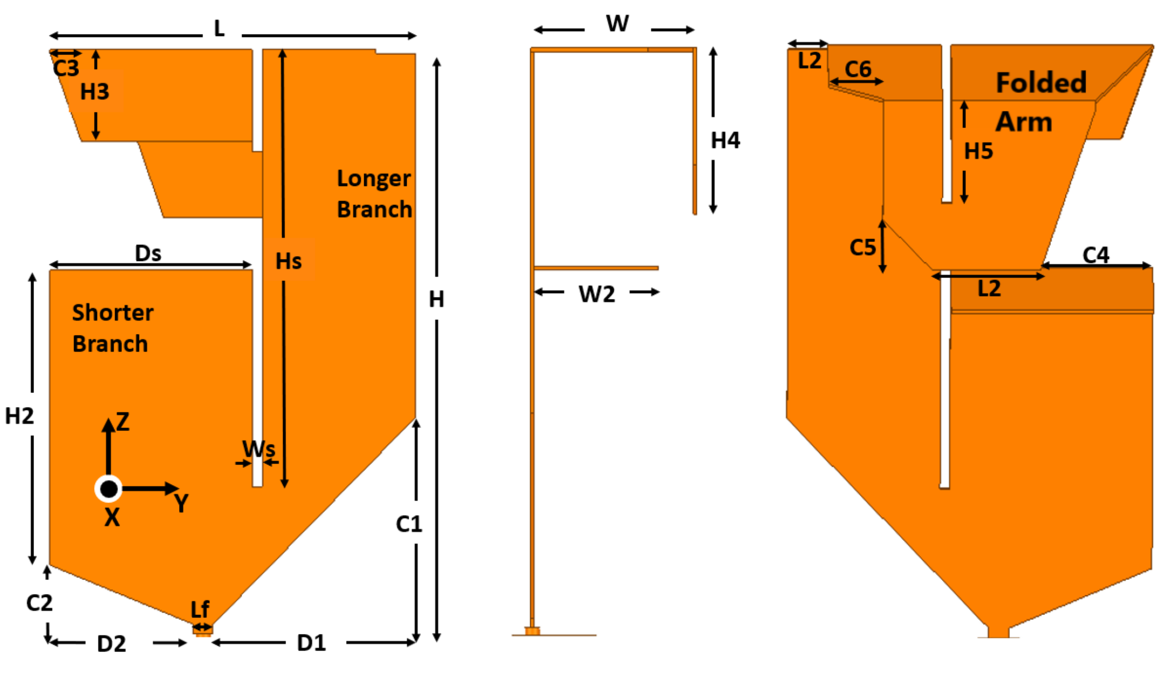

(a) Front View (b) Side View (c) Back View

Figure 3.1 Proposed monopole antenna geometry. (a) Front View. (b) Side View. (c) Back View.

Table 3.2 Detailed Dimensions of the folded Monopole

Parameter	Value (mm)
H	58
L	37
W	17
W2	13
Ws	1
H2	30
H3	9.5
H4	17
H5	10
Hs	44
L2	11
Lf	2
D1	20.5
D2	14.5
Ds	20.5
C1	22
C2	7
C3	3
C4	11.5
C5	5
C6	5.5

The proposed monopole antenna was simulated and optimized using ANSYS HFSS. To investigate more on how the antenna covers the required frequency bands, the antenna current distribution is shown in Figure 3.2 for three different frequencies. For the low band center frequency (788MHz), the highest current intensity followed the slot on the long branch as shown by black lines in the front and back views in Figure 3.2. The current path length with the highest intensity is measured to be 97mm which is very close to the quarter wavelength at 788MHz (95mm), and this explains the role of the slot in the proposed antenna miniaturization. For the higher band which starts at 1559 MHz, the current path length on the short branch can be calculated by C2+H2+W2 which is 50mm and this is almost equals to the quarter wavelength at 1559MHz (48mm). The short branch is responsible for the higher band resonance from 1559 to 5925MHz.

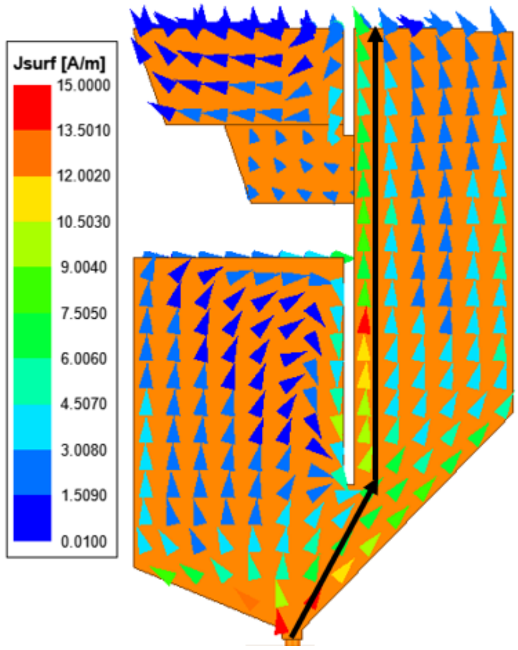

(a) 788MHz (Front View)

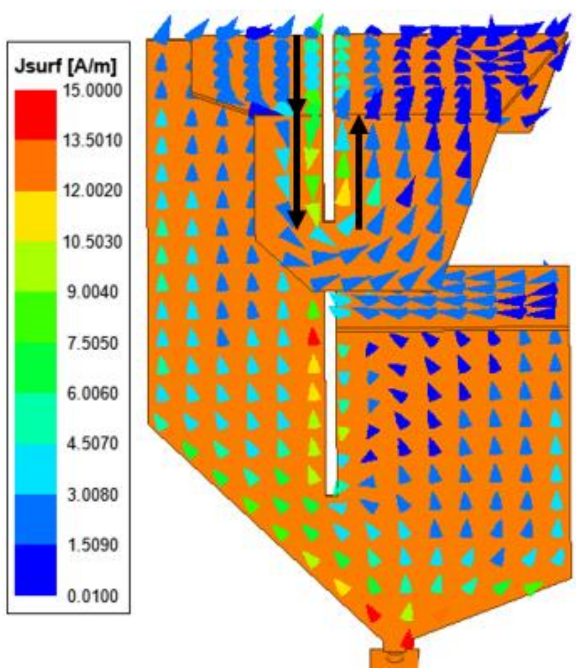

(b) 788MHz (Back View)

Figure 3.2 The proposed monopole antenna current distribution. (a) 788MHz (Front View). (b) 788MHz (Back View). (c) 1559MHz. (d) 5900MHz.

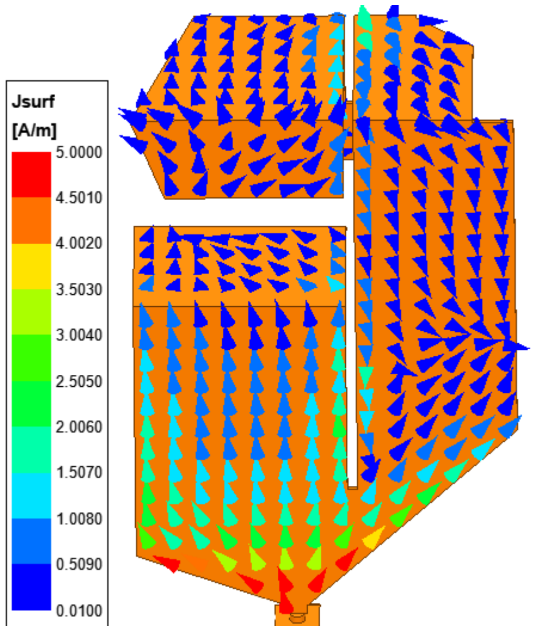

(c) 1559MHz

Figure 3.2. Continued.

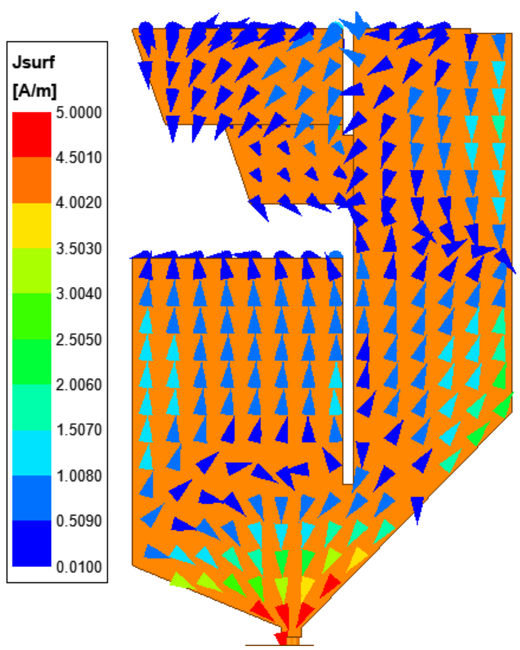

(d) 5900MHz

Figure 3.2. Continued.

3.3 Antenna Equivalent Circuit Model

To develop an equivalent circuit model for the proposed antenna, the antenna simulated VSWR with its geometry will be used. The circuit model is derived from the simulated VSWR using the techniques presented in [37]. Figure 3.3 shows the proposed monopole antenna equivalent lumped element circuit model, it consists of three main parts to represent the antenna short branch, long branch, and slot. The slot separates the antenna low band and high band and acts as a band stop filter around 1220MHz, this represented by an LC resonator to ground and a capacitor C2 in series. The antenna long branch which is responsible for the antenna's low band resonance is represented by an RLC parallel band pass filter with center frequency of 775MHz. The short branch is modeled by two parallel RLC band pass filters as the short branch is responsible for the wide high band from 1559 to 5925MHz which requires two band pass filters to cover it. The antenna equivalent circuit model is simulated and tuned using Advanced Design System (ADS). Figure 3.4 shows the VSWR for the circuit model and for the antenna HFSS simulation which shows a good agreement, this agreement proves that the circuit model represents the antenna accurately.

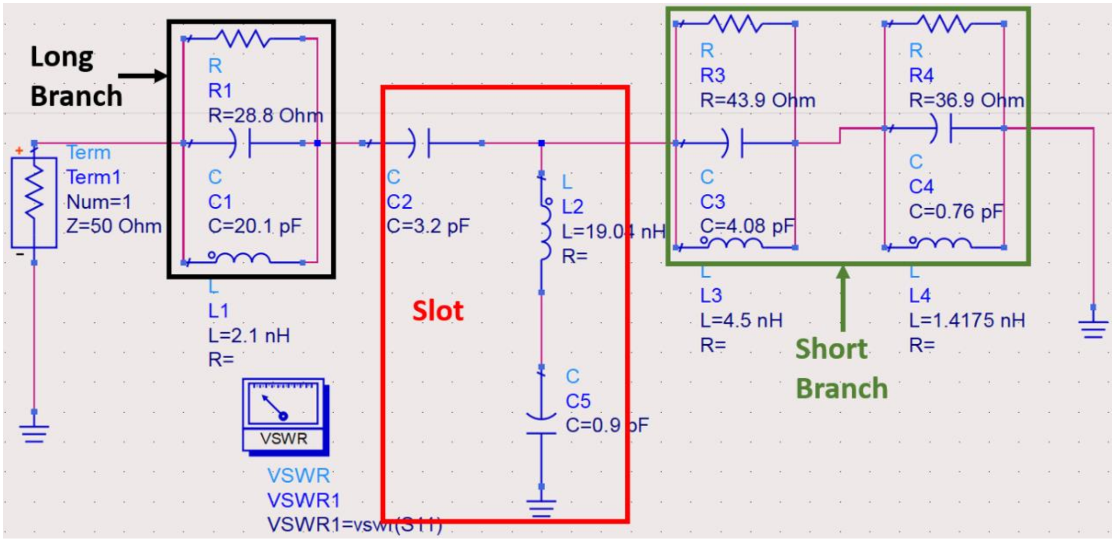

Figure 3.3 Equivalent circuit model of the antenna.

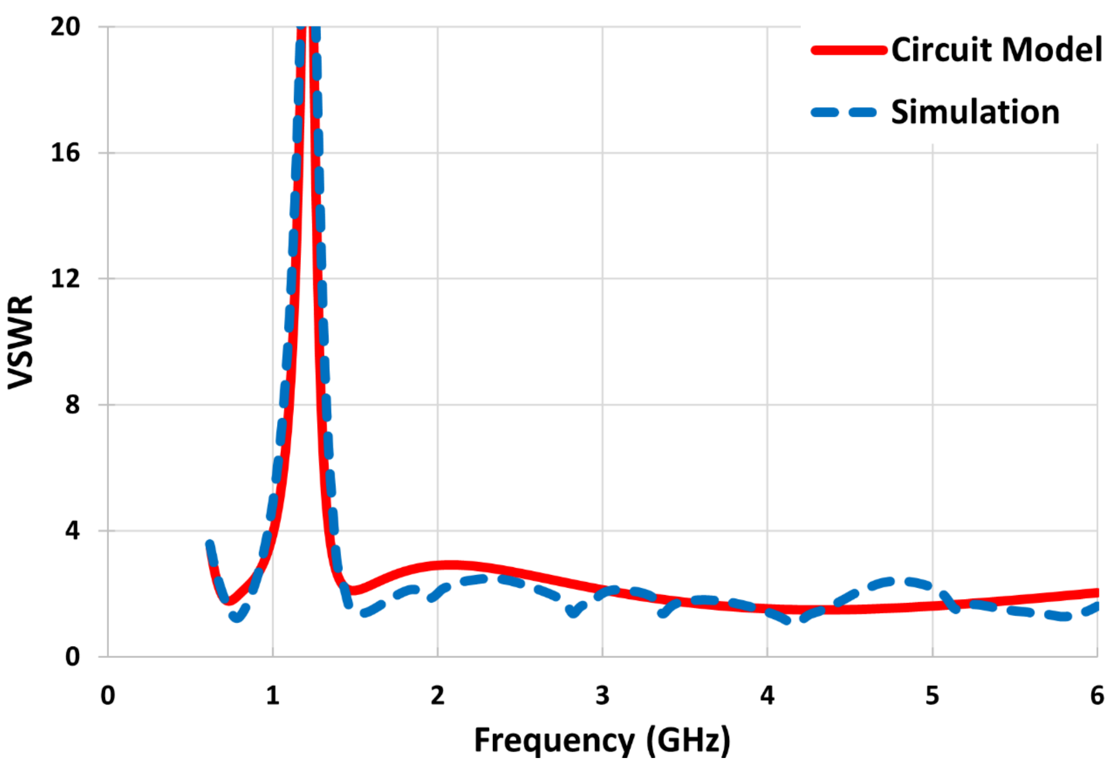

Figure 3.4 Simulated and circuit model driven VSWR of the antenna.

3.4 Antenna Parametric Sweeps

Parametric studies on the antenna slot width and length and on the top two folded long branch portions were conducted to observe their effects on the antenna resonance. The parametric sweeps were conducted when all the other parameters values are the same as in Table 3.2. Figure 3.5 shows the effect of the slot width Ws on the antenna VSWR when Ws changed from 1 to 3 mm. Increasing slot width Ws increases the current path and this results in lowering the resonance frequency for both the low band at 617MHz and the high band at 1559MHz, when Ws is 3mm, the VSWR at 617MHz is 2.7 compared to 3.3 when the VSWR is 1mm while at 960MHz the opposite effect to 617MHz is observed. At 1559MHz, increasing Ws shifts the resonance frequency lower which is the same effect as for 617MHz. Changing the slot length Hs affects both the low band and the high band due to increasing the current path for both the long and short antenna branches as shown in Figure 3.6. To conclude on the effect of the slot on the antenna resonance, slot width and length affect antenna low band and high band, increasing the slot width or length shifts the resonance frequency lower at 617MHz and at 1559MHz. On the other hand, decreasing the slot width or length shifts the resonance frequency higher.

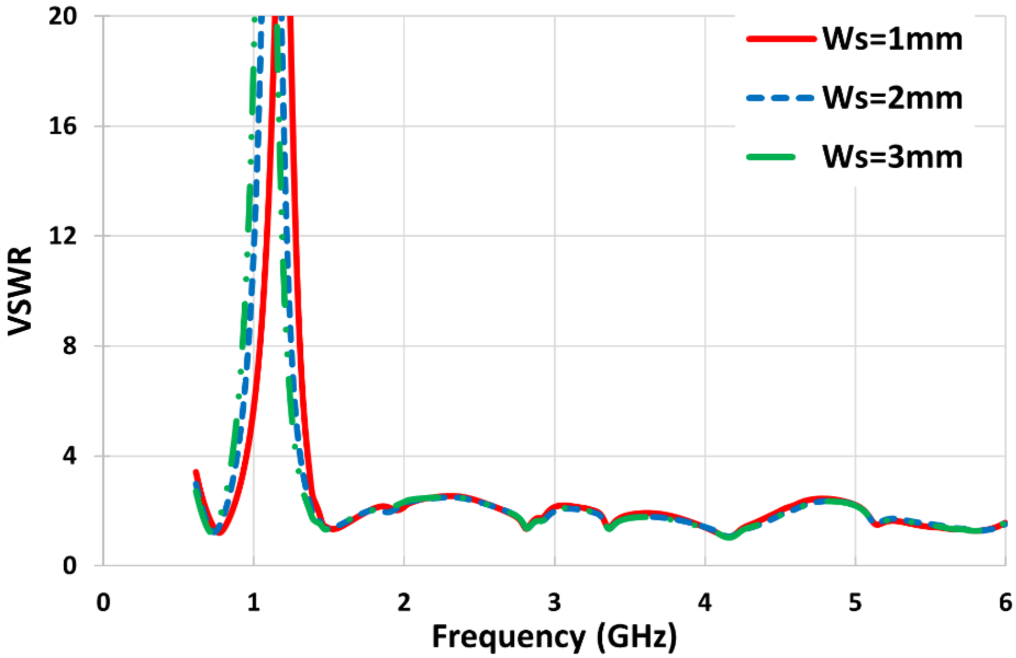

Figure 3.5 Effect of the slot width (Ws) on the antenna VSWR.

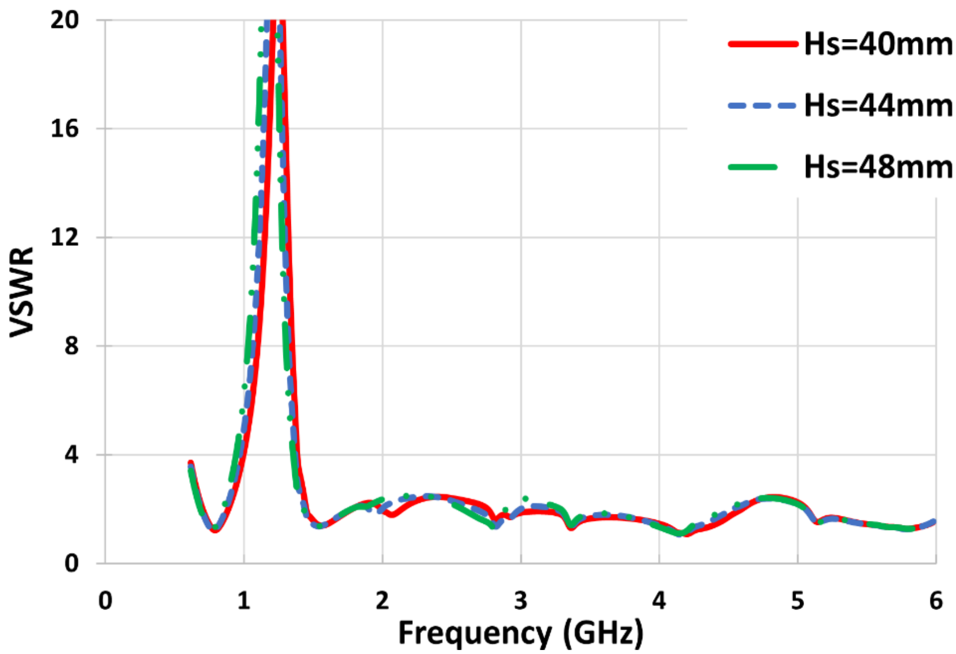

Figure 3.6 Effect of the slot length (Hs) on the antenna VSWR.

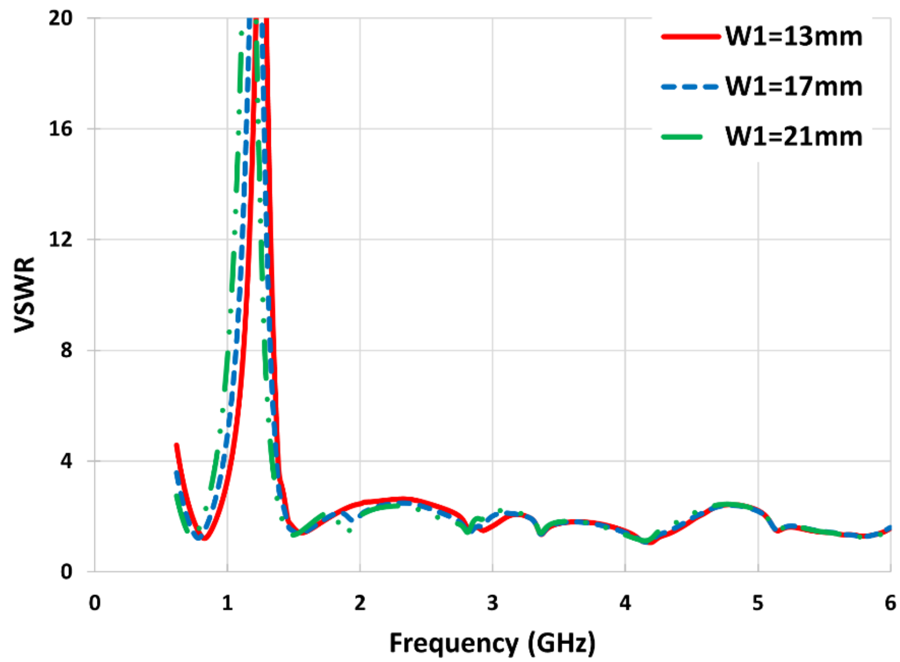

Figure 3.7 Effect of the long branch horizontal folded arm width (W1) on the antenna VSWR.

Figure 3.7 shows the effect of the long branch horizontal folded arm width (W1) on the antenna VSWR. Changing W1 affects the low band at 617 and 960MHz, increasing W1 shifts the low band resonance frequency lower while decreasing W1 shifts the low band resonance frequency higher. Figure 3.8 shows the effect of the long branch vertical folded arm height (H4) on the antenna VSWR. Changing H4 mainly affects the low band, increasing H4 shifts the low band resonance frequency lower and decreasing H4 shifts the low band resonance frequency higher which is the same effect as changing W1. When increasing H4 to be larger than 20mm, it starts affecting the higher band at 1559MHz due to the coupling between long and short branches as the distance between both branches will be small.

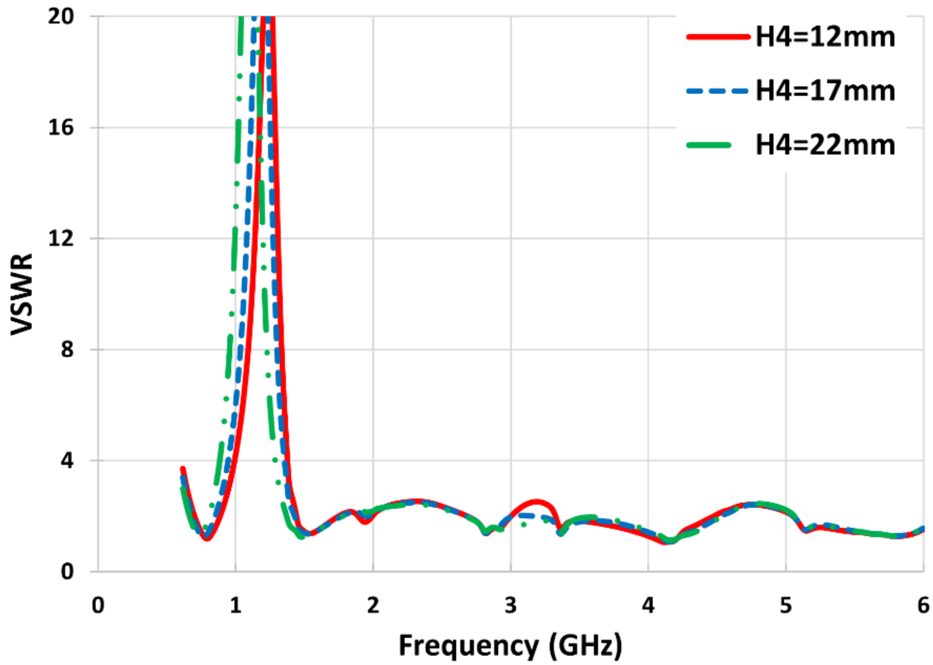

Figure 3.8 Effect of the long branch vertical folded arm height (H4) on the antenna VSWR.

3.5 Antenna Prototype and Measurements

A prototype for the proposed antenna is fabricated and measured on a one-meter diameter rounded ground plane as well as on vehicle's roof as shown in Figure 3.9. The antenna VSWR is measured on one-meter ground plane and then compared to the antenna simulated VSWR as shown in Figure 3.10. Both simulated and measured VSWR met the antenna VSWR requirements listed in Table for all frequency bands. A good agreement is also achieved between the measured and simulated VSWR as shown in Figure 3.10.

The fabricated antenna prototype radiation characteristics is measured with a MVG Satimo chamber on a ground plane and then on a vehicle. In the next sub-sections, the far field measurements are discussed for 5G sub-6GHz, LTE, V2X, and GNSS.

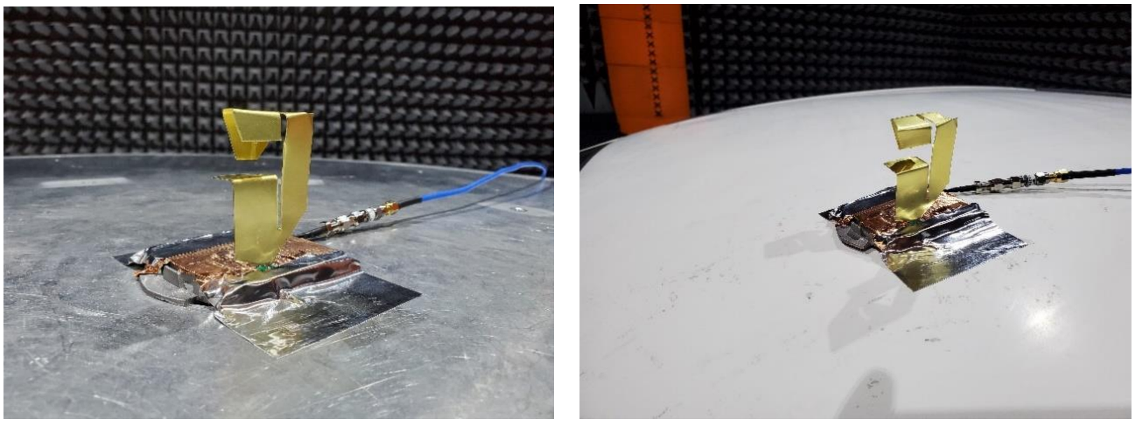

(a) ground plane (b) vehicle's Roof

Figure 3.9 Fabricated antenna prototype. (a) On ground plane. (b) On vehicle's Roof.

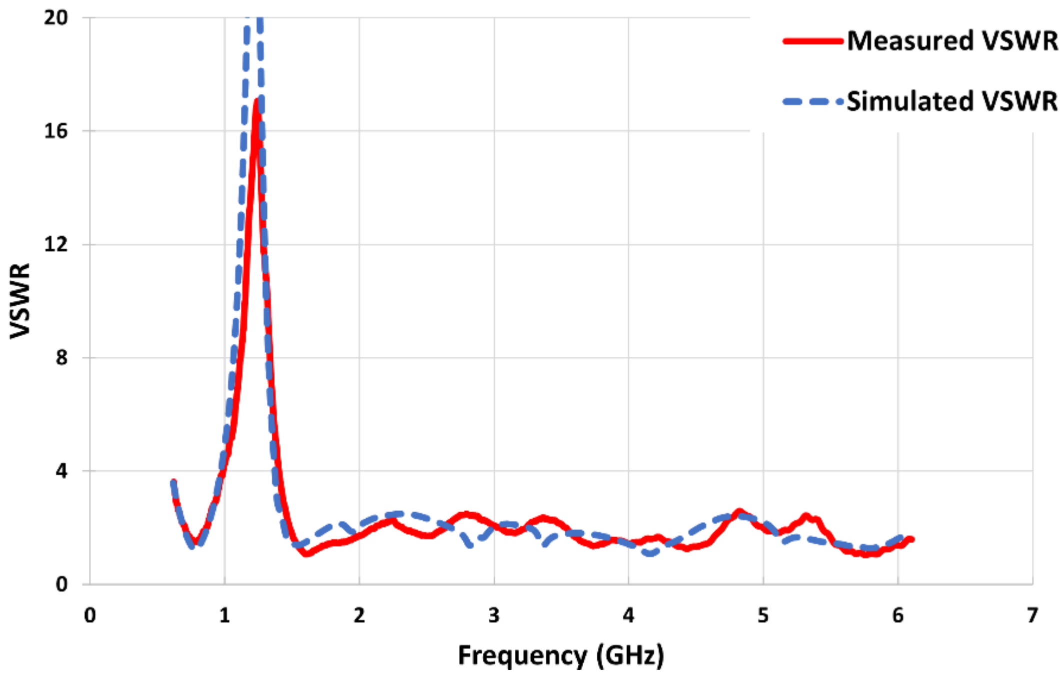

Figure 3.10 The proposed antenna simulated and measured VSWR.

<u>3.5.1 5G Sub-6GHz Far-Field Measurements</u>

It is important for the cellular antenna to have an omni-directional coverage when mounted on a vehicle roof. This omnidirectional radiation is essential in the elevation angles from 75° to 87° (15° to 3° above horizon). Figure 3.11 shows a comparison of horizontal cuts of the proposed antenna vertically polarized gain between simulation on a ground plane, measurements on ground plane and on vehicle's roof at 80° elevation angle at frequencies of 788, 2300, 3300, and 5000MHz. For the low band at 788MHz, the antenna's radiation pattern is omni-directional with a good agreement between simulation and measurements. At 2300 and 3300MHz, the radiation started to be directive especially in the measurements on both the vehicle and the ground plane. At 5000MHz, the radiation pattern is more directive to the back and front of the antenna. The vehicle's roof curvature affects the radiation pattern at 5000MHz as some ripples and reflections started to appear.

In the automotive industry, the antenna gain is expressed in linear average gain (LAG) which can be calculated using the following steps: (1) Measure the vertically polarized gain in linear units for 13 elevation angles from 75° to 87° at each of the 360° azimuth angles. (2) Calculate the average azimuth gain for each of the 13 elevation angles. (3) Calculate the average gain in linear units from the 13 elevation angles to get one gain value for each frequency and then convert to logarithmic scale (dBi). Figure 3.12 shows the measured LAG on ground plane and a vehicle. For the low band, the LAG is above -1 dBi for both measurements on the ground plane and vehicle while the middle band is above 1.5 dBi. After 4GHz, the LAG is lower due to the reflections that appeared in the 5000MHz radiation pattern. The proposed antenna LAG meets the LAG requirements listed in Table for the ground plane and vehicle measurements.

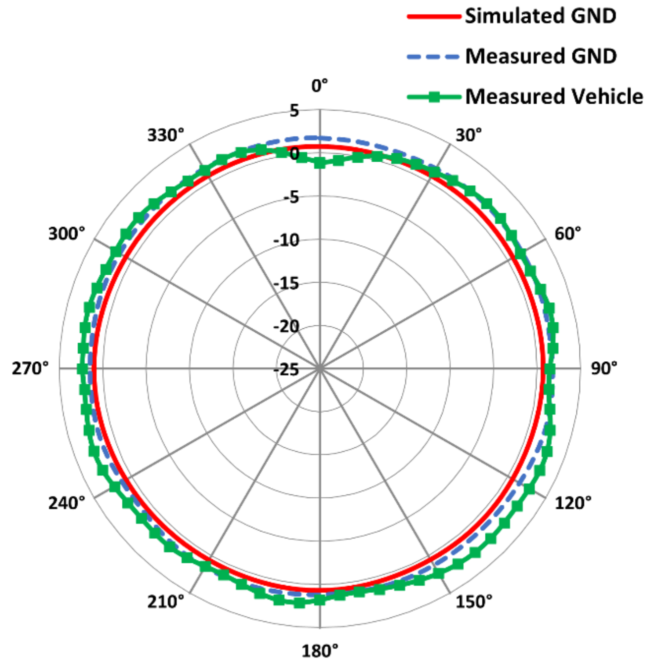

(a) 788MHz

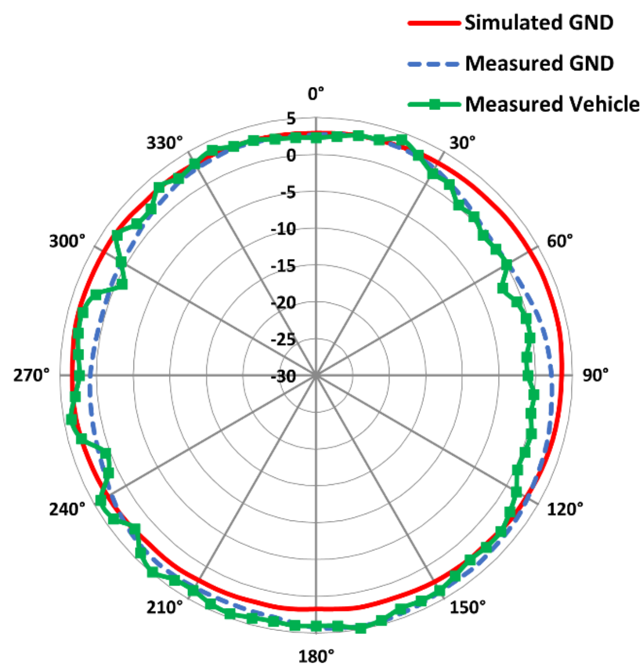

(b) 2300MHz

Figure 3.11 The antenna cellular radiation pattern simulated on ground plane and measured on ground plane and a vehicle at 80° elevation angle (0° is the direction of the front of the vehicle). (a) 788MHz. (b) 2300MHz. (c) 3300MHz. (d) 5000MHz.

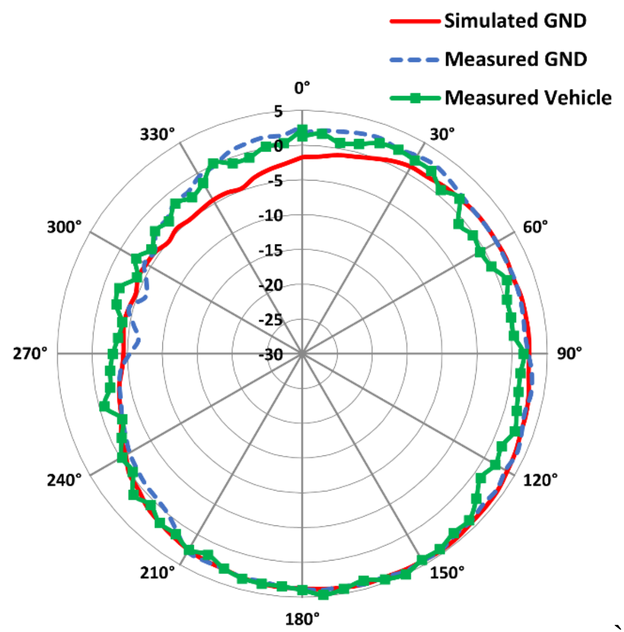

(c) 3300MHz

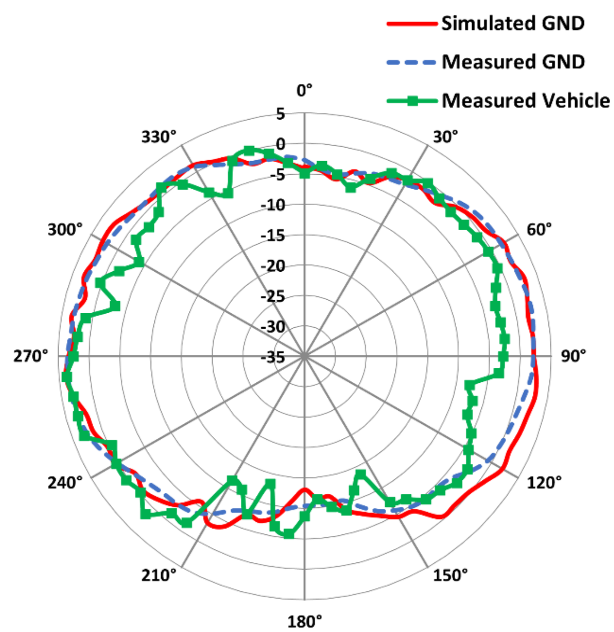

(d) 5000MHz

Figure 3.11. Continued.

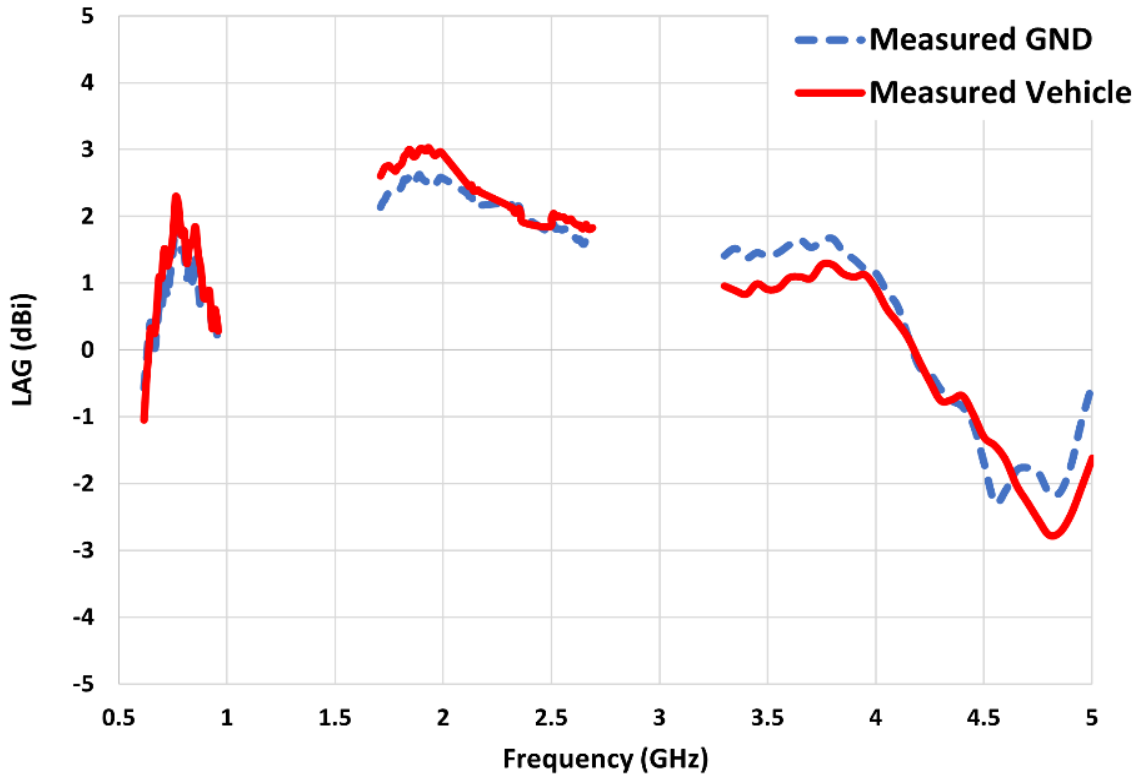

Figure 3.12 5G and LTE measured LAG on a ground plane and a vehicle.

Figure 3.13 shows the antenna 5G and LTE measured efficiency on a ground plane and on a vehicle, the efficiency followed the same curve trend as the LAG curve. For the low band, the efficiency is more than 50% and more than 60% for the high band for both measurement's conditions.

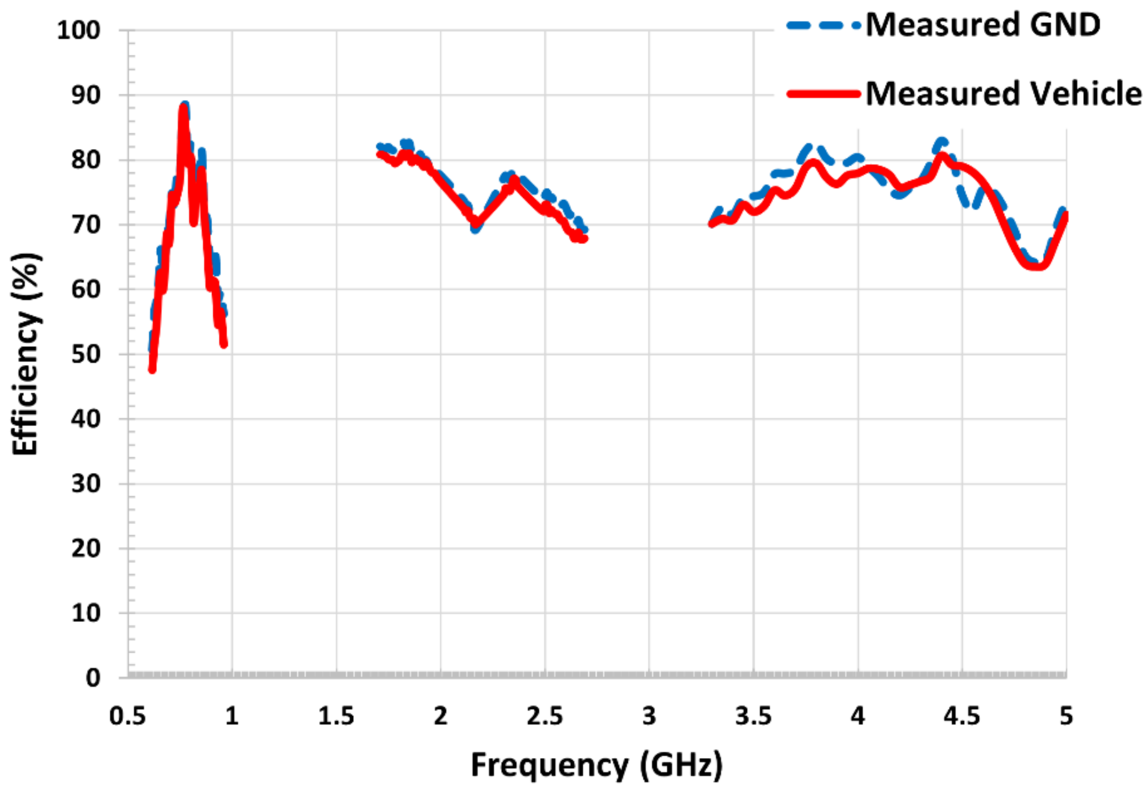

Figure 3.13 5G and LTE measured efficiency on a ground plane and a vehicle.

3.5.2 V2X Far-Field Measurements

Omni-directional coverage is also important for V2X in elevation angles from 80° to 96°. Figure 3.14 shows the antenna vertically polarized gain radiation pattern at 5900MHz and 90° elevation (Horizon) when simulated on ground plane, measured on ground plane, and measured on a vehicle. The measured radiation pattern has a good omni-directional coverage with maximum gain of 3 dBi and minimum gain of -7 dBi when measured on a vehicle and a maximum gain of 0 dBi and a minimum gain of -5 dBi when measured on a ground plane.

The antenna V2X LAG is calculated following the same steps written in the previous sub-section except the V2X elevation angles are from 80° to 96°. Figure 3.15 shows the V2X measured LAG on ground plane and on a vehicle, the measured LAG on a vehicle is lower than the measured LAG on a ground plane due to the roof curvature. The antenna meets the V2X LAG requirements listed in Table 3.1. Figure 3.16 shows the V2X measured efficiency on a ground plane and a vehicle. The measured efficiency is above 70% for the whole V2X bandwidth.

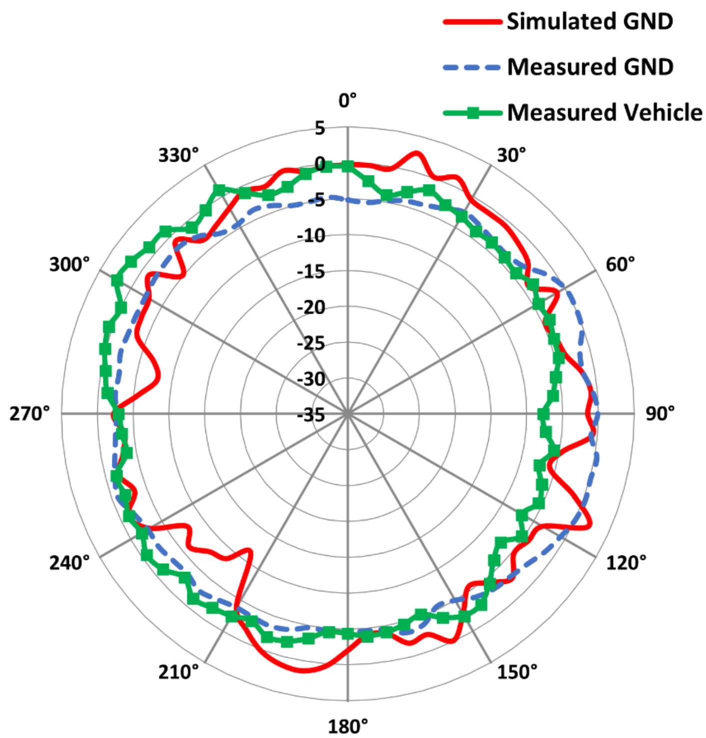

Figure 3.14 The antenna V2X radiation pattern simulated on ground plane and measured on ground plane and a vehicle at 90° elevation angle at 5900MHz (0° is the direction of the front of the vehicle).

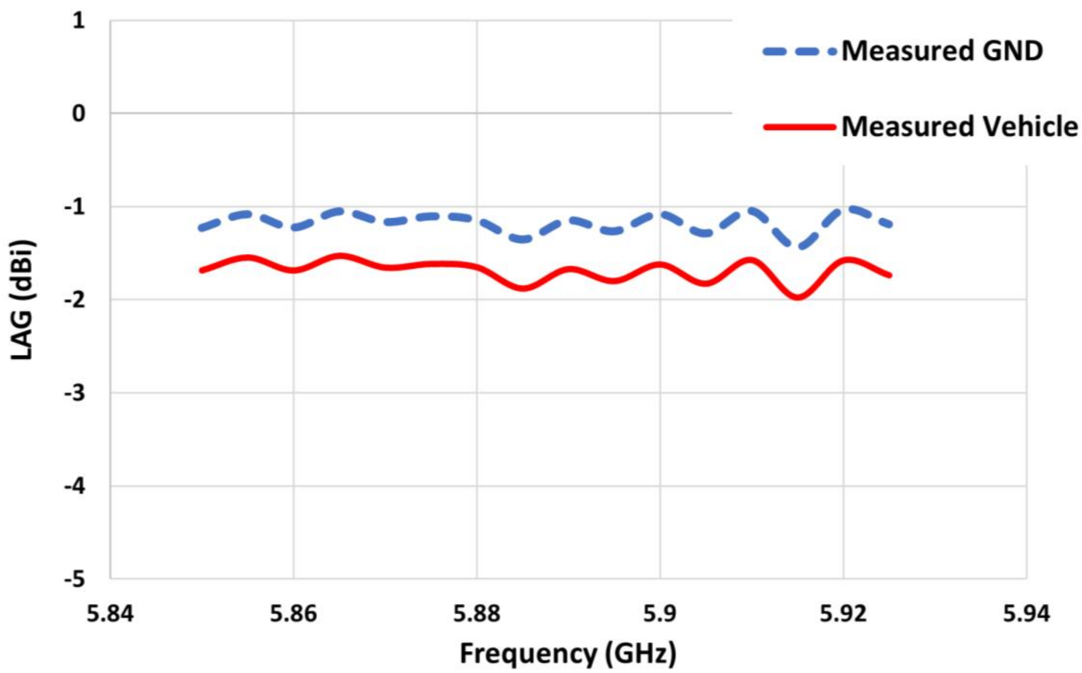

Figure 3.15 V2X measured LAG on a ground plane and a vehicle roof.

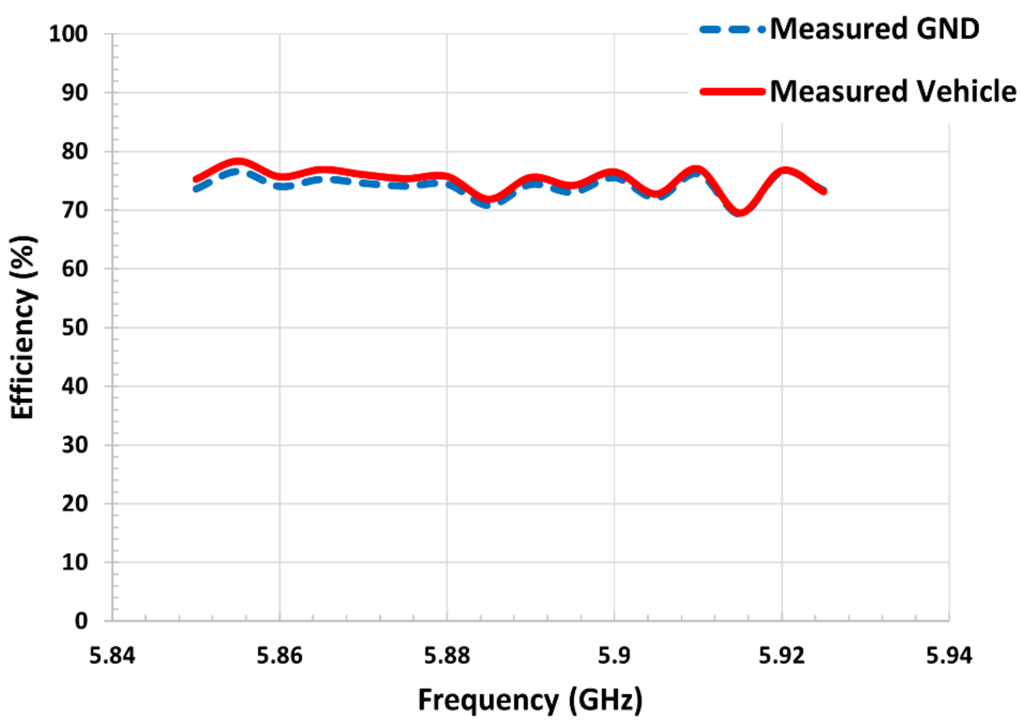

Figure 3.16 V2X measured efficiency on a ground plane and a vehicle roof.

3.5.3 GNSS Far-Field Measurements

Although the monopole antenna is linearly polarized, GNSS measurements were conducted, and the measurements are presented in right hand circular polarization (RHCP). The targeted GNSS frequency bands are BEIDOU B1 (1559.04 - 1563.16MHz), GPS L1 and GALILEO E1 (1574.42 - 1576.42MHz) and GLONASS G1 (1597 – 1606MHz). Figure 3.17 shows two vertical cuts (XZ and YZ planes) for the measured GNSS passive RHCP gain at 1575MHz when mounted on a vehicle and on aground plane. The two vertical cuts didn't show any nulls. The antenna RHCP gain at zenith is -9 dBc and the gain increases until it reaches 0 dBc around 45°. Monopole antennas have low gain at zenith and when converting the linear polarized gain to RHCP gain, another 3 dBi is subtracted and this is the reason its RHCP gain at zenith is -9 dBc.

To check the antenna GNSS coverage, horizontal cuts for four different elevation angles (10°, 20°, 30°, 40°) measured on ground plane at 1575MHz are shown in Figure 3.18. The proposed antenna shows good radiation pattern without major nulls in angles of interest; however, the antenna has better coverage to the front of the antenna (azimuth angles from 0° to 180°) than to the back of it (azimuth angles from 180° to 360°).

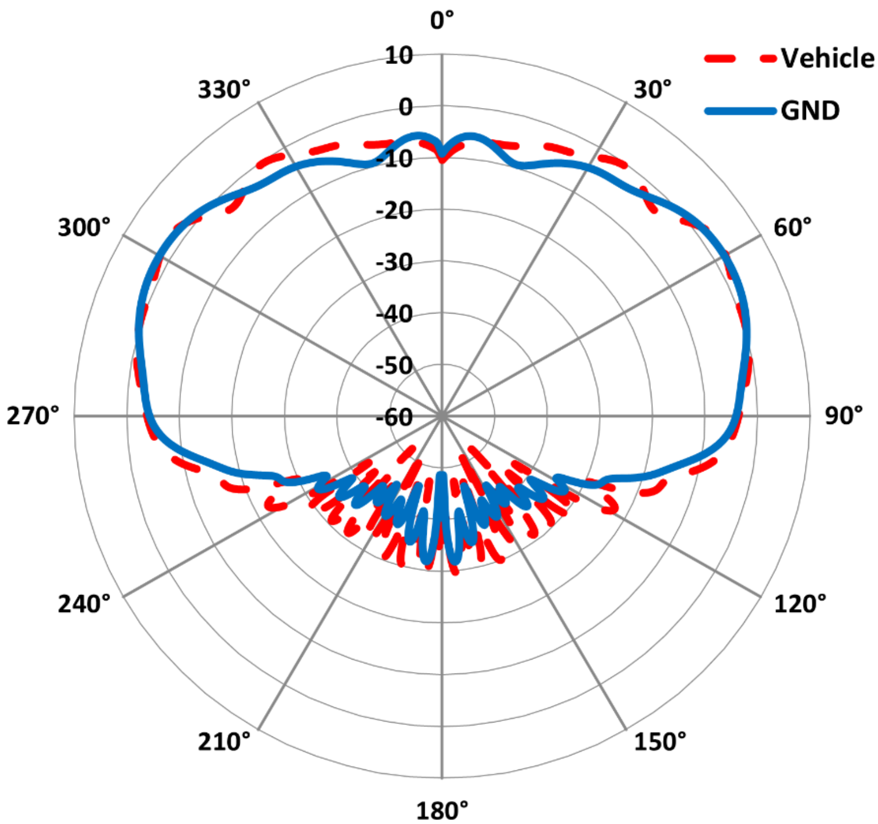

(a) XZ plane (Ø=90°)

Figure 3.17 GNSS Passive RHCP gain in the XZ and YZ planes at 1575MHz measured on ground plane and vehicle. (a) XZ plane (Ø=90°). (b) YZ plane (Ø=0°).

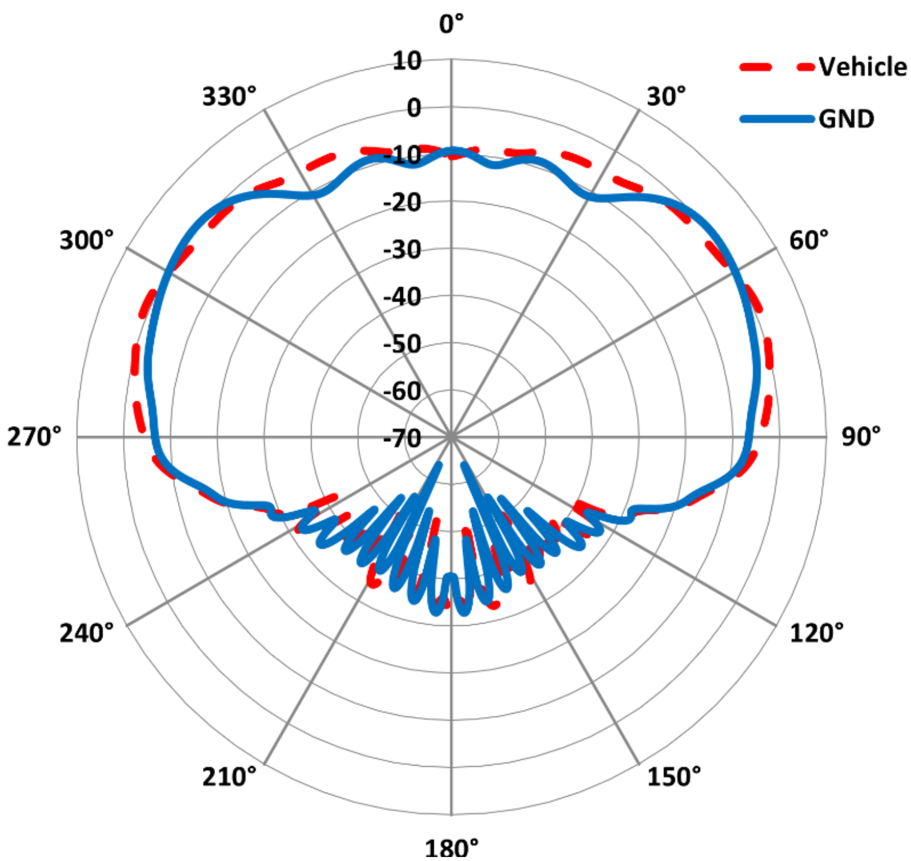

(b) YZ plane (Ø=0°)

Figure 3.17. Continued.

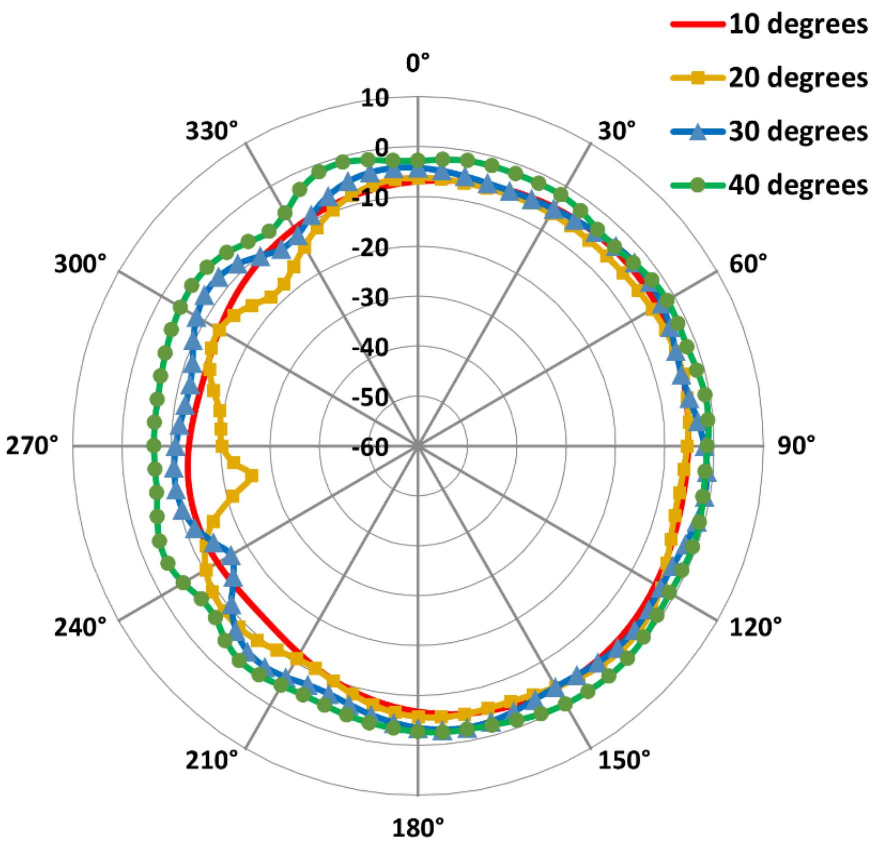

Figure 3.18 Measured GNSS radiation pattern for 4 different elevation angles at 1575MHz on a ground plane.

To measure the antenna active performance, low noise amplifier (LNA) is constructed using two LNA stages of signal processing LNA-00120 connected to a Qualcomm GNSS Saw Filter (B4327) to provide the required isolation as shown in Figure 3.19. Figure 3.20 shows the S21 of the constructed LNA which has a gain of 28 dB in the GNSS frequency band and a good isolation in the other bands. The LNA has the same gain as an automotive grade GNSS LNA gain.

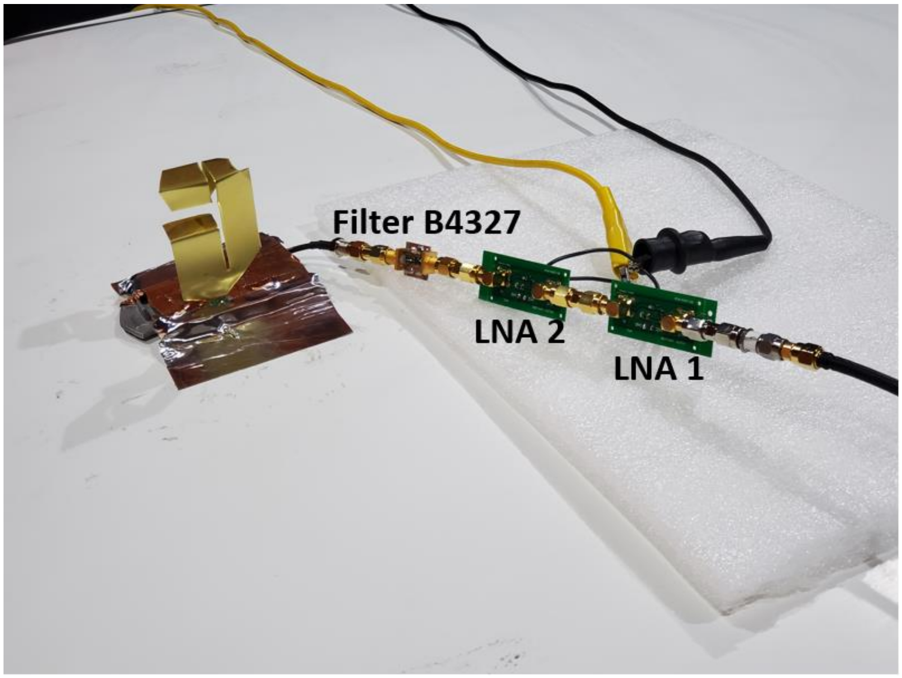

Figure 3.19 GNSS active antenna measurements setup on a vehicle.

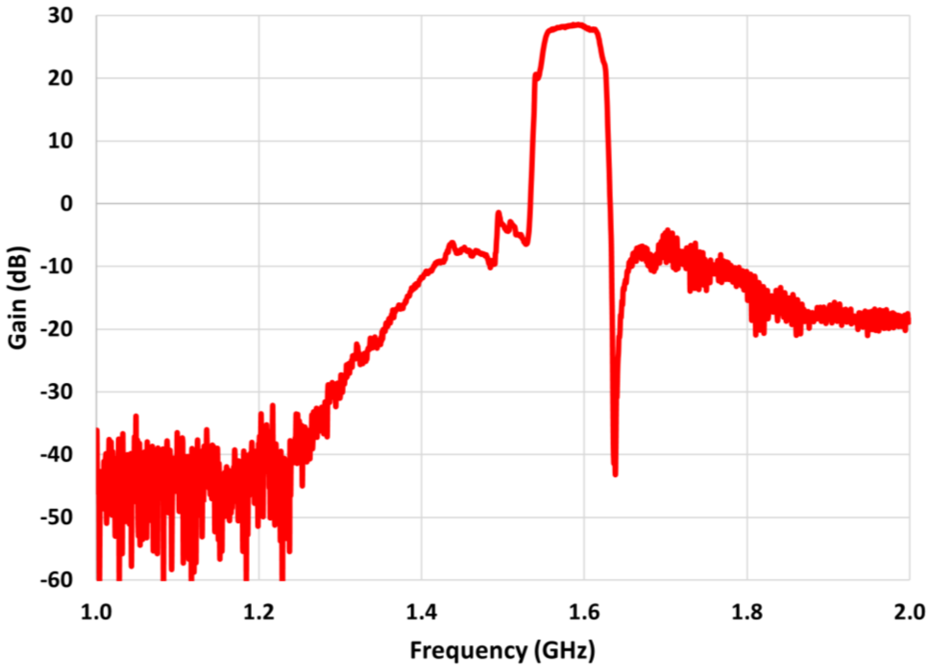

Figure 3.20 Final LNA gain.

Figure 3.21 shows the measured GNSS active RHCP LAG on a vehicle at the center frequencies of BEIDOU, GPS, and GLONASS which are 1561, 1575, and 1601MHz, respectively. The LAG is calculated for each elevation angle by averaging azimuth angles. The active RHCP LAG is more than 20 dBc for most of the elevation angles considering using an LNA with normal gain value for automotive industry. This shows that the proposed antenna can receive GNSS signals with acceptable gain despite the antenna's dominant linear polarization. Adding GNSS to the antenna makes the antenna design challenging as the antenna long branch can block the GNSS signal if not designed carefully and this is the reason for the chamfering and tapering in the upper folded parts of the antenna long branch.

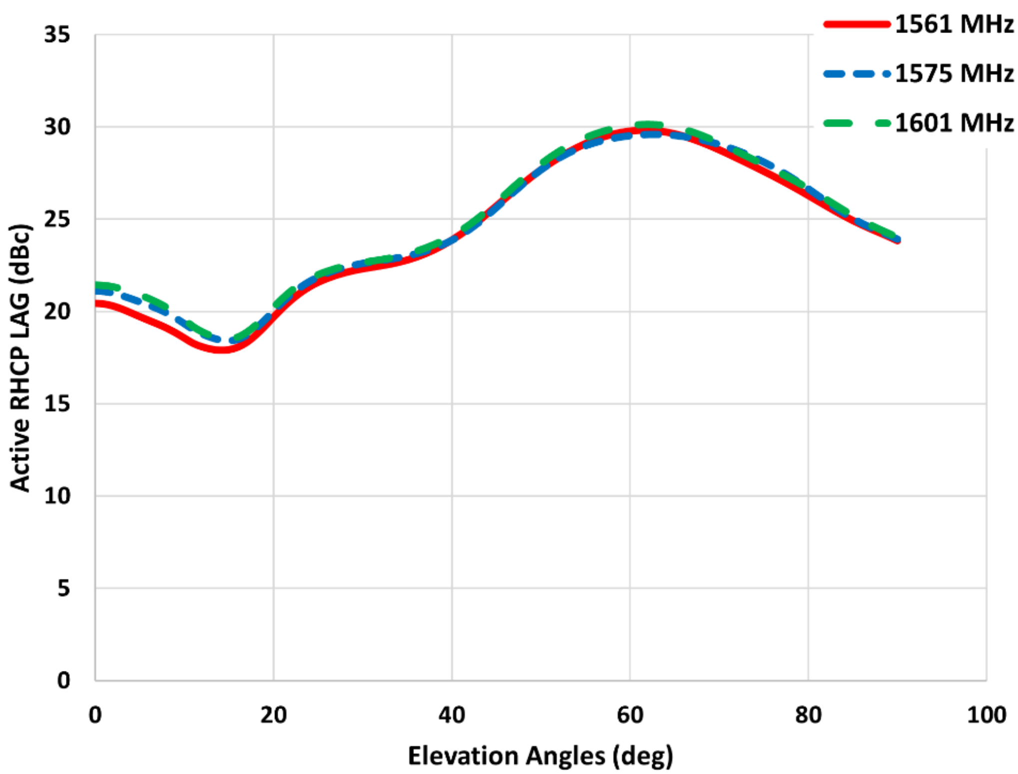

Figure 3.21 Measured GNSS active RHCP LAG on a vehicle.

3.6 Conclusions

In this chapter, the design of a compact multi-band folded monopole antenna is presented. The antenna is designed to cover 5G sub-6GHz, LTE, GNSS higher frequency band, and V2X. The proposed antenna is a three-dimensional monopole antenna with two branches to cover the enlarged bandwidth required which starts from 617MHz to 6GHz. The antenna is simulated, optimized and then a prototype is fabricated and measured on one-meter ground plane and on a vehicle roof. The antenna measurements are expressed in terms of VSWR, radiation pattern, LAG, and efficiency in which the presented antenna showed good results that met the performance requirements. The proposed antenna has measured efficiency of 50-90% in the operating frequency and LAG of -2.2 to 3 dBi across the entire frequency band. A good agreement is achieved between the simulated and measured results. The antenna is optimized to enhance the GNSS performance and the active RHCP LAG is measured which was more than 20 dBi in most of elevation angles using normal 28 dB automotive GNSS LNA.

CHAPTER FOUR

ANALYSIS OF C-V2X ANTENNA PERFORMANCE ON VEHICULAR PANORAMIC GLASS

Antenna placement on vehicles significantly impacts the antenna performance, so most antennas are placed on the vehicle's roof to avoid signal blockage by the vehicle's metallic parts. Automakers are always improving the aesthetic design of the cars to meet the growing market demand and to cope with the competition from other car manufacturers. One of the aesthetic improvements is the introduction of full glass roof which changes the roof structure from the conventional metallic roof to a glass roof. The full glass roof must protect the car passengers from sun radiation and outside condition so materials other than glass are added to the glass roof such as tint layers.

In this chapter, the effects of the full glass roof on the C-V2X antenna will be studied by a series of measurements and then the C-V2X antenna performance degradation when mounted on glass roof will be investigated. At the end of this chapter, suggestions to improve the performance of the C-V2X antenna on glass will be discussed.

4.1 C-V2X Antenna Performance on Vehicle's Glass Roof

Figure 4.1 shows a vehicle's glass roof section provided by an automotive Original Equipment Manufacturer (OEM) with its CAD files. No other information is provided by the OEM or the glass supplier about the construction of the glass roof or the layer stacked inside the glass. The glass roof section consisted of a metal frame underneath the glass and the rear mirror on which the antenna was mounted, as shown in Figure 4.1. The glass size (LxWxH) is 982x620x3.85mm^3 with the antenna mounting hole located 125mm from the back end of the glass. The quarter-wavelength C-V2X monopole antenna is used in this study as the monopole is the most used C-V2X antenna in the automotive industry. The monopole antenna has height of 13mm and width of 2mm as shown in Figure 4.2. The antenna is soldered to a PCB with an FR4 material which has dielectric constant of 4.4. Small green cable with SMA connector is then soldered to the antenna to act as the antenna feed. The antenna and the PCB were mounted on a small shark-fin chassis with a size (LxW) of 117x67mm^2, as shown in Figure 4.2.

First, the C-V2X monopole antenna is measured when mounted on the 1-meter metallic ground plane and then mounted on the vehicle's glass roof, as shown in Figure 4.3. The far-field measurements data is analyzed and the expressed in two parameters, i.e., Radiation Pattern (RP) and Linear Average Gain (LAG). The RP is measured at three elevation angles of (10, 0, -6), corresponding to theta angles of 80°, 90° (Horizon), and 96°, respectively, at 5.9GHz. These elevation angles are chosen to represent above horizon (80°), horizon (90°) and below horizon (96°) angles. LAG is calculated by converting the measured gain values in dBi to linear values at each elevation angle between Ө=80° to Ө=96°, at each of the 360 azimuth points per elevation. The linear values are then averaged and converted back to dBi to determine the LAG value for each frequency. The angular resolution is 1° and 2° for theta and phis resulting in 16 theta points and 181 phi points per elevation point.

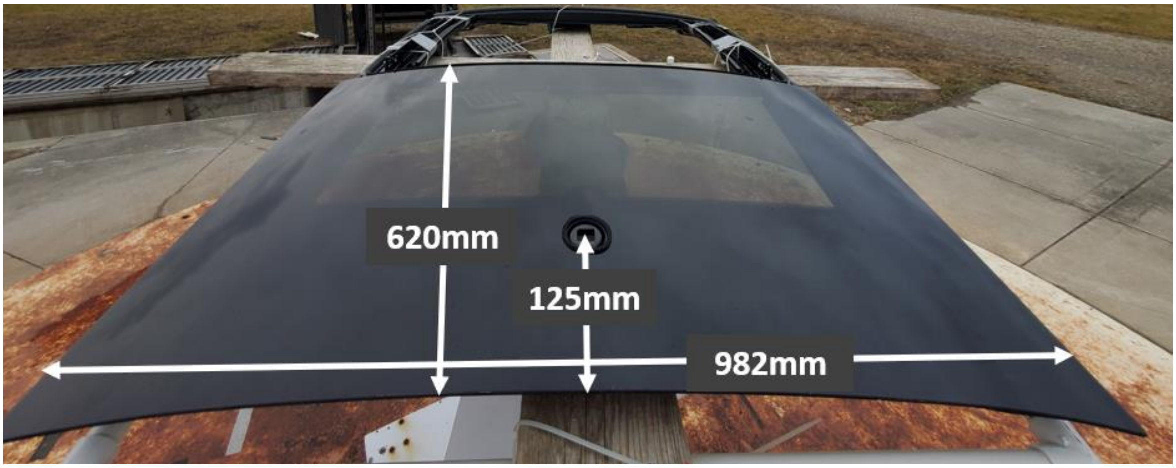

Figure 4.1 Vehicle's glass roof section dimensions.

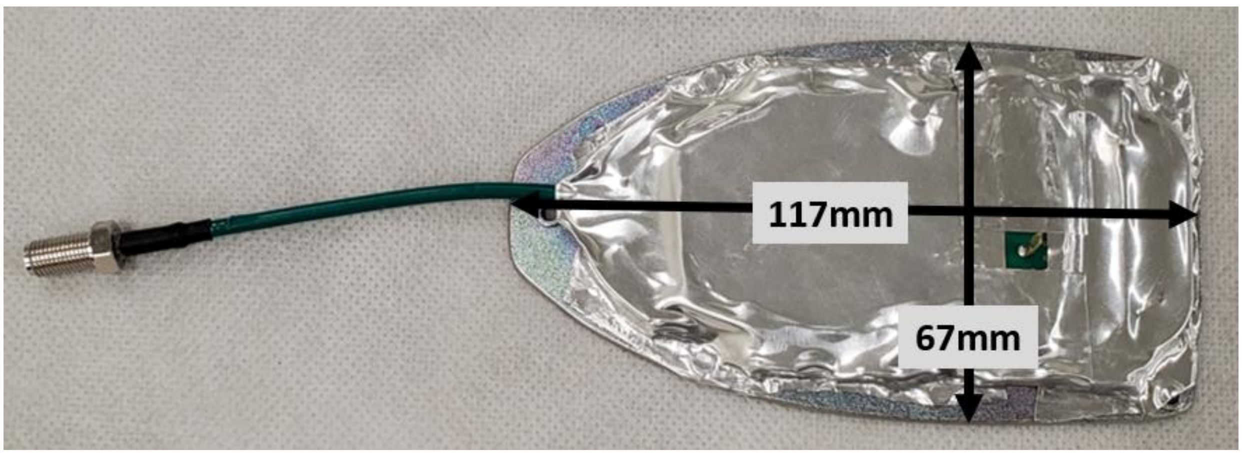

Figure 4.2 C-V2X monopole antenna prototype used in the study.

(a) Vehicle's glass roof (b) 1m metallic ground plane

Figure 4.3 C-V2X monopole antenna when mounted on (a) Vehicle's glass roof. (b) 1 m metallic ground plane (GND).

Figure 4.4 shows the performance comparison for the C-V2X monopole antenna when mounted on the metallic ground plane vs. mounted on the vehicle's glass roof. When mounted on metal, the antenna has an omnidirectional radiation pattern without nulls at all three elevation angles. In contrast, when the monopole was mounted on the glass roof, the radiation pattern had deep nulls on the sides at Ø=90° and 270°. The front and back directions of the radiation pattern don't show deep nulls like the side directions; however, the gain is significantly less than the metallic ground plane placement. The antenna performance degradation when mounted on the vehicle's glass roof is evident in the LAG shown in Figure 4.5, as the LAG for the monopole mounted on metal is about -1 dBi compared to -9 dBi when mounted on the glass roof.

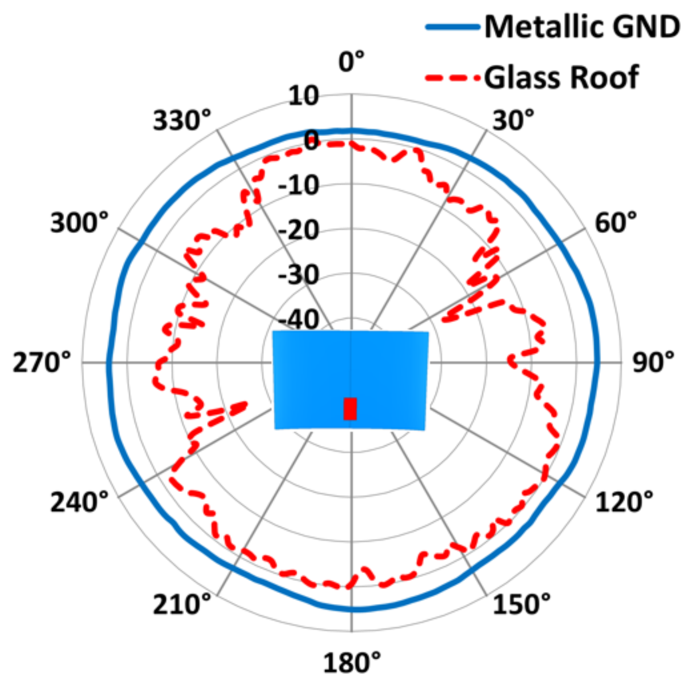

(a) Theta=80°

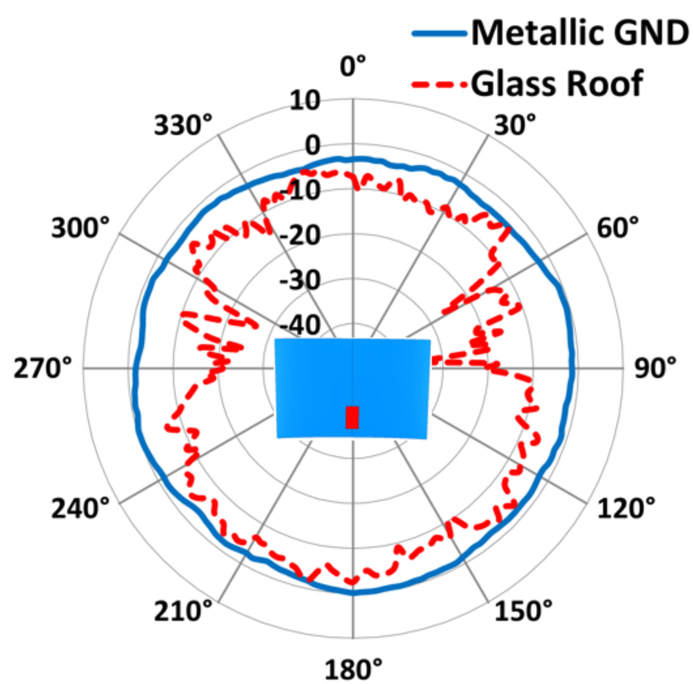

(b) Theta=90°

Figure 4.4 C-V2X monopole antenna measured radiation pattern on the full glass roof and metallic GND at 5.9 GHz. (a) Theta=80°. (b) Theta=90°. (c) Theta=96°.

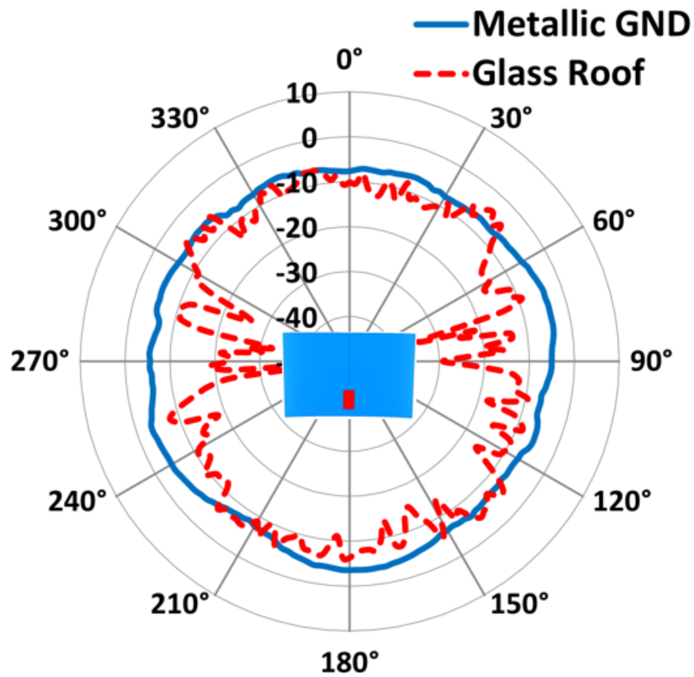

(c) Theta=96°

Figure 4.4 Continued.

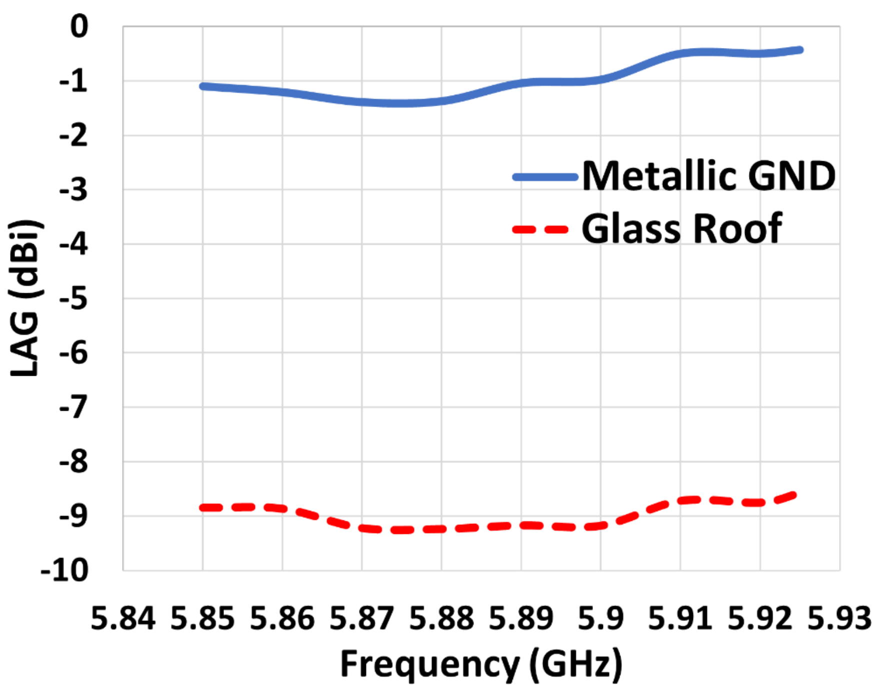

Figure 4.5 C-V2X monopole antenna measured LAG on the full glass roof and metallic GND.

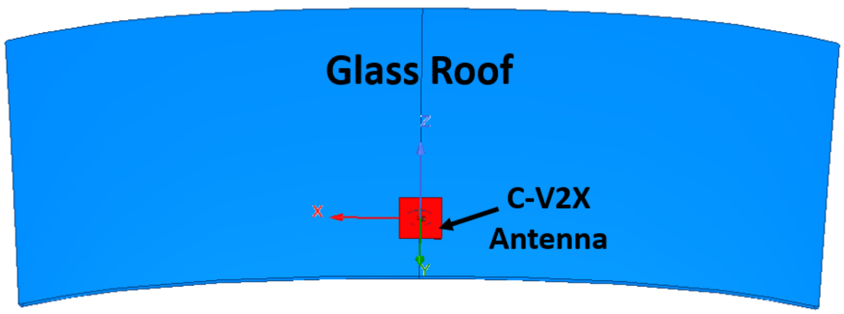

Figure 4.6 C-V2X monopole simulation on clear glass roof.

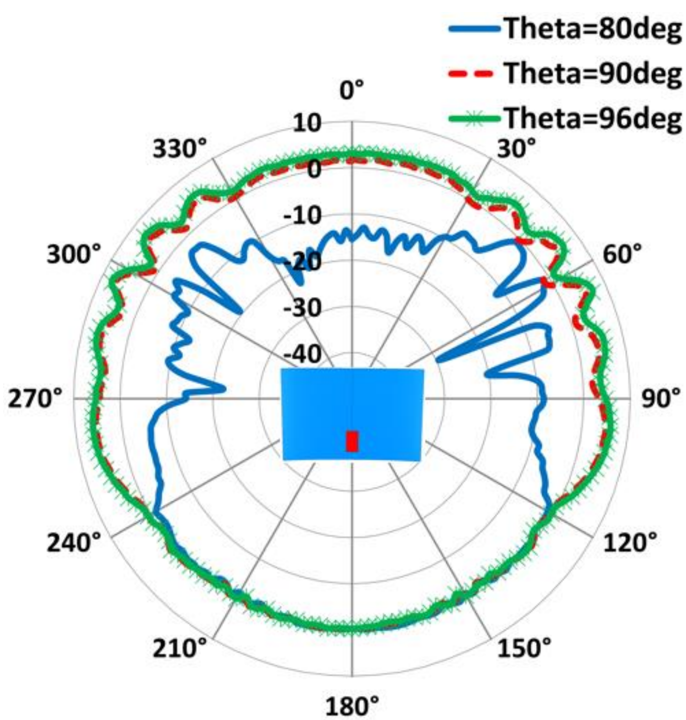

Figure 4.7 C-V2X monopole antenna simulated Radiation pattern on the glass roof at 5.9 GHz.

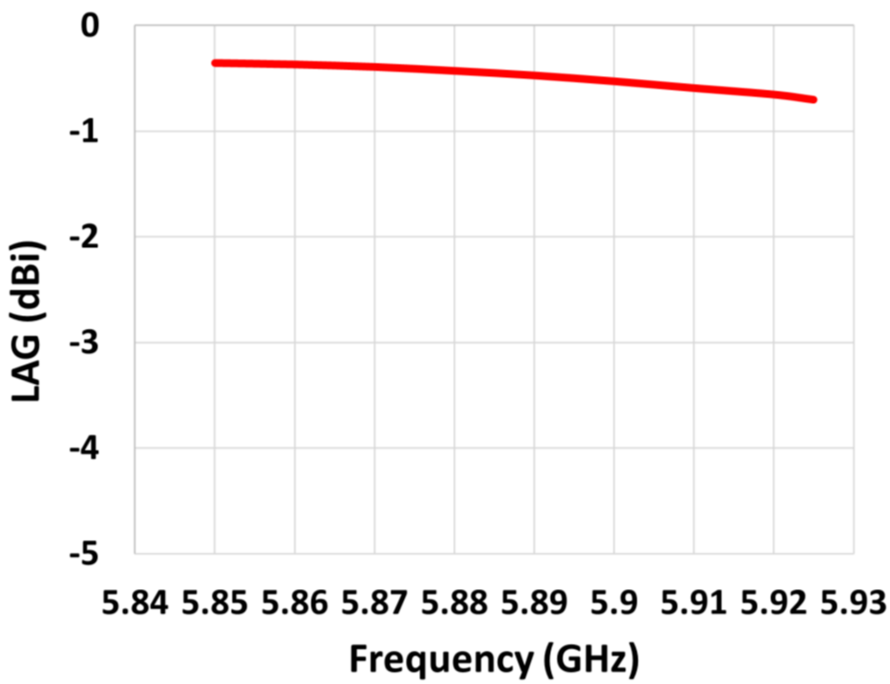

Figure 4.8 C-V2X monopole antenna simulated LAG on the glass roof.

To better understand the results in Figure 4.4, simulations of the C-V2X monopole antenna on the full glass roof were performed to investigate the reasons behind the performance degradation. Ansys HFSS finite element method (FEM) was used for the simulation with the glass roof CAD files (Figure 4.6). Glass material was assigned a dielectric constant of 7 and a dielectric loss tangent of 0.009 [33]. The simulation results don't match the measurements as shown in Figure 4.7 and Figure 4.8 as the simulated RP shows void of deep nulls, which are missing in measured results, and simulated LAG is more than eight dBi higher than the measurements, which indicates that there are materials other than the glass causing the antenna performance degradation on the full glass roof.

4.2 C-V2X Dipole Antenna Performance on Vehicle's Glass Roof

Although the C-V2X monopole antenna is the most used antenna in the automotive industry, a half wavelength C-V2X dipole antenna is also added to the measurements campaign to study the effect of the vehicle glass roof on different antenna type. The dipole antenna is suitable to be investigated as it is less dependent on the ground plane than the monopole antenna. The C-V2X dipole antenna is measured when mounted on 1-meter metallic ground plane and then mounted on the vehicle's glass roof as shown in Figure 4.9. The far-field measurements data is analyzed and the expressed in two parameters, i.e., Radiation Pattern (RP) and Linear Average Gain (LAG) as in the monopole antenna case which discussed earlier.

(a) 1m metallic ground plane (b) Vehicle's glass roof

Figure 4.9 C-V2X dipole antenna when mounted on (a) 1 m metallic ground plane (GND). (b) Vehicle's glass roof.

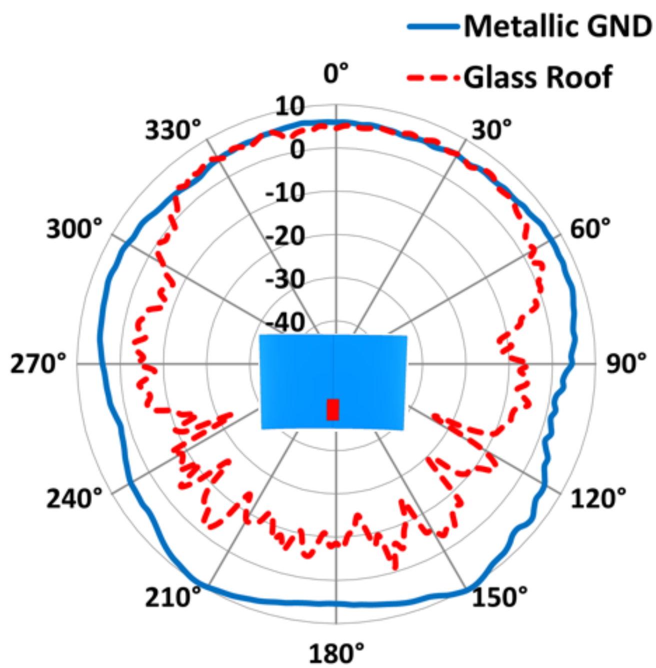

(a) Theta=80°

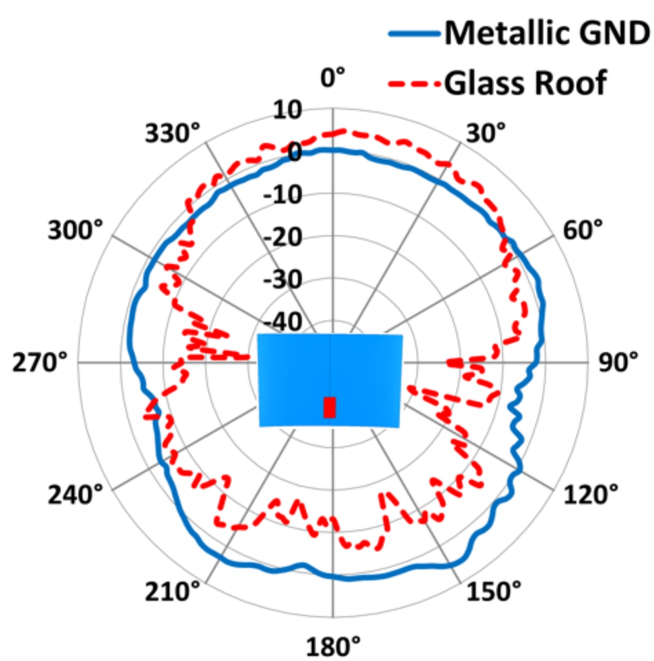

(b) Theta=90°

Figure 4.10 C-V2X dipole antenna measured radiation pattern on the full glass roof and metallic GND at 5.9 GHz. (a) Theta=80°. (b) Theta=90°. (c) Theta=96°.

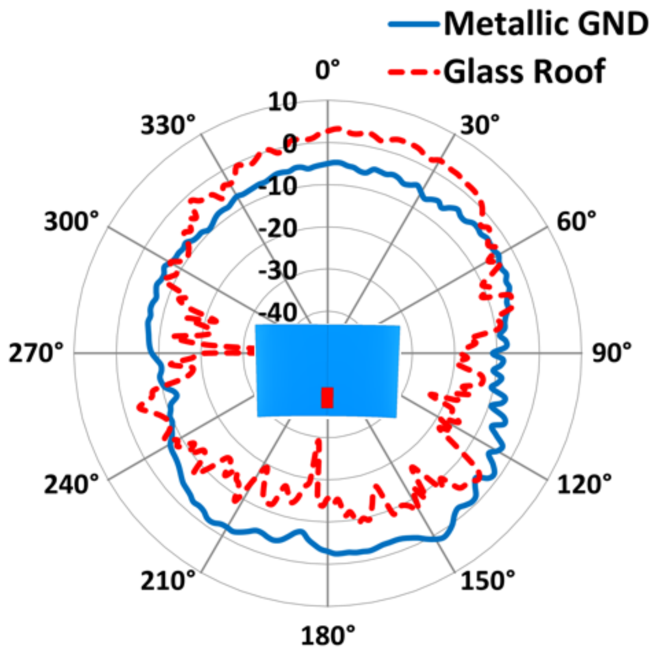

(c) Theta=96°

Figure 4.10 Continued.

Figure 4.10 shows the performance comparison for the C-V2X dipole antenna radiation pattern when mounted on the metallic ground plane vs. mounted on the vehicle's glass roof. When mounted on metal, the antenna has an omnidirectional radiation pattern without nulls at all three elevation angles. In contrast, when the dipole was mounted on the glass roof, the radiation pattern had deep nulls. The front and back directions of the radiation pattern don't show deep nulls like the side directions; however, the gain is less than the metallic ground plane placement. The antenna performance degradation when mounted on the vehicle's glass roof is evident in the LAG shown in Figure 4.11, as the LAG for the dipole mounted on metal is about 1 dBi compared to -6.5 dBi when mounted on the glass roof. The C-V2X dipole antenna followed the same trend as the C-V2X monopole antenna when mounted on the vehicle’s glass roof which indicates the antenna performance degradation when mounted on the vehicle's glass roofs is not related to the antenna type.

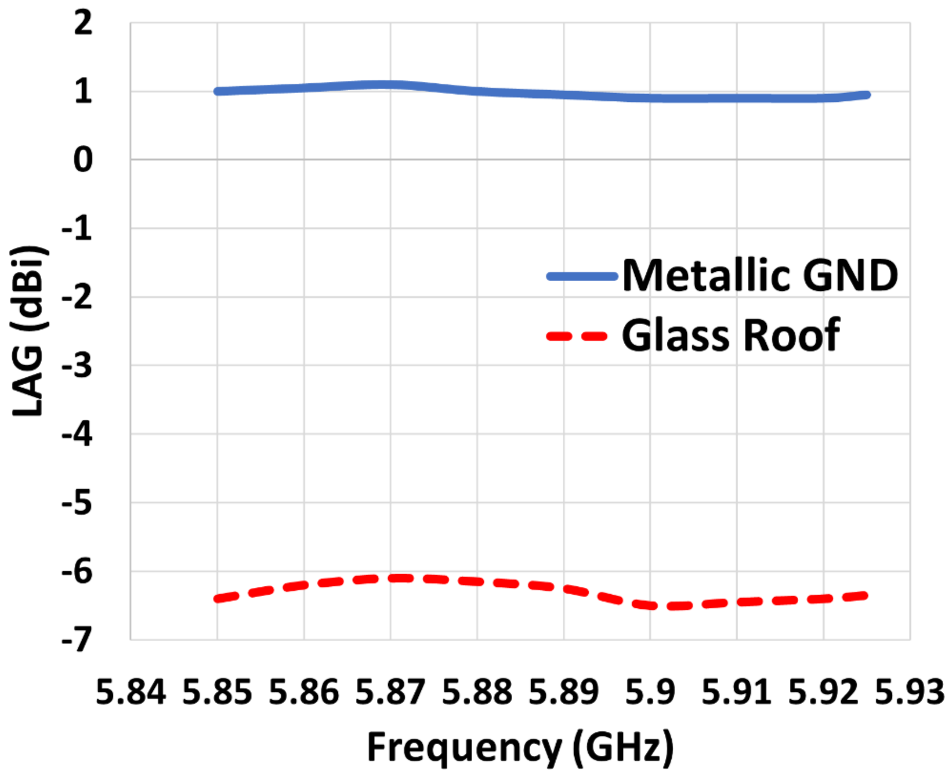

Figure 4.11 C-V2X dipole antenna measured LAG on the glass roof and 1m metallic GND.

4.3 C-V2X Antenna Measurements on Different Glass Types

As it is quite clear that the glass properties affect the antenna performance, different studies were performed and presented in this section to learn further the effect of roof material properties on antenna performance. The C-V2X monopole antenna was measured on four different glass types.

- Clear Glass Sheet with the size of 508x508x3.2mm^3.
- Low Emissivity (Low E) Glass Sheet with the size of 508x508x3.2mm^3.
- Metal Wire-Reinforced Glass Sheet with the size of 585x585x6.35mm^3.

- Vehicle's glass roof sample.

(a) Clear Glass

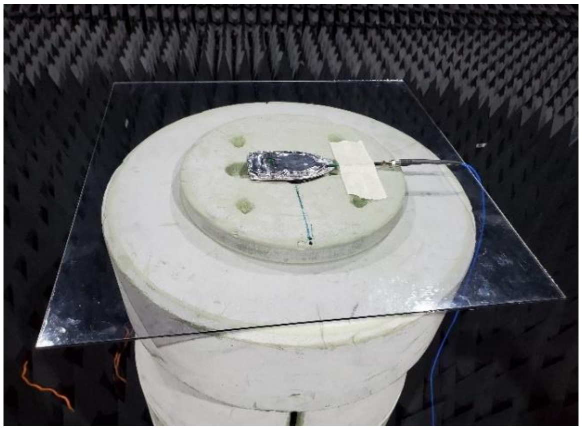

(b) Low E Glass

(c) Wire Reinforced Glass

(d) Vehicle's Glass Roof

Figure 4.12 C-V2X monopole antenna when measured on (a) Clear Glass. (b) Low E Glass. (c) Wire Reinforced Glass. (d) Vehicle's Glass Roof.

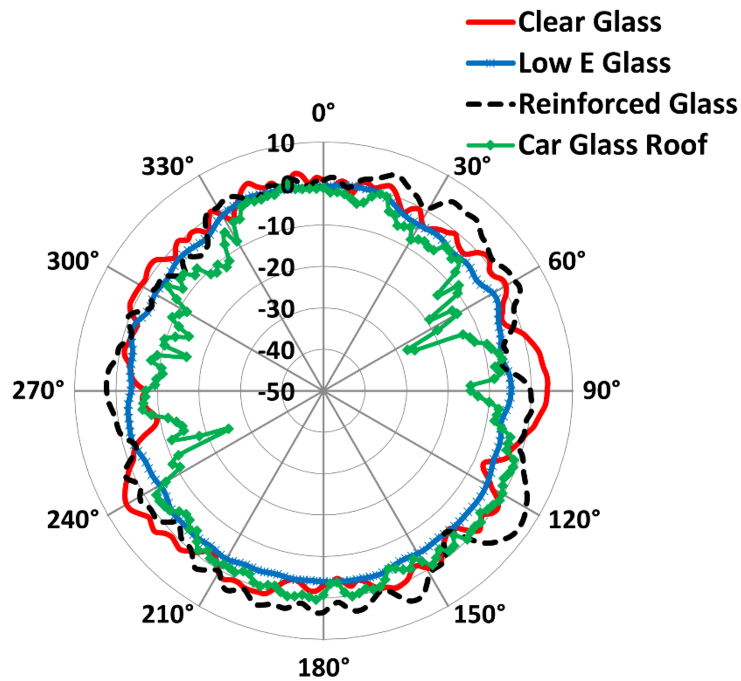

(a) Theta=80°

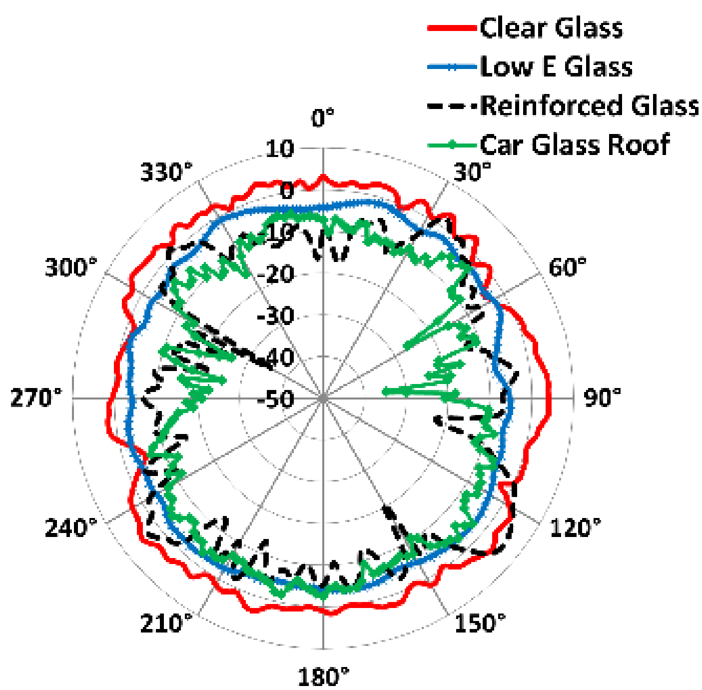

(b) Theta=90°

Figure 4.13 C-V2X antenna radiation pattern measured on different glass materials. (a) Theta=80°. (b) Theta=90°. (c) Theta=96°.

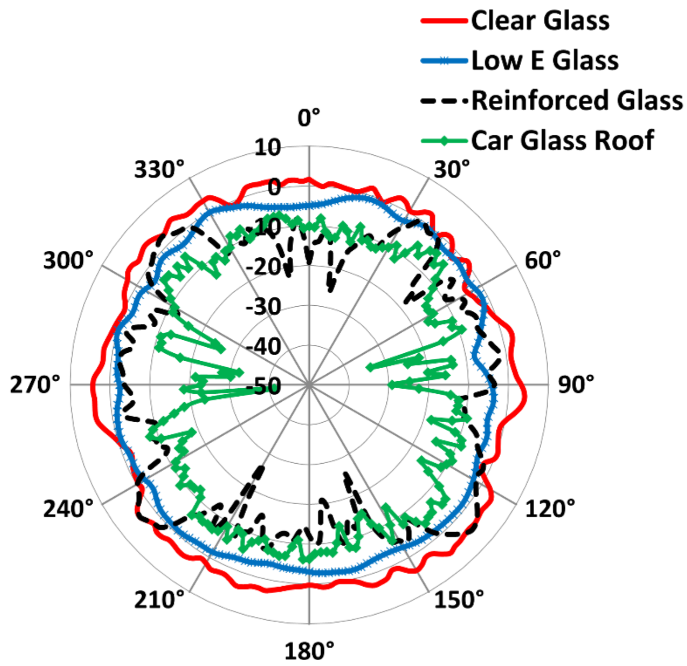

(c) Theta=96°

Figure. 4.13 Continued.

Figure 4.12 shows the measurement setup for the C-V2X monopole antenna when mounted on the four types of glass. Figure 4.13 shows the radiation pattern and LAG for the C-V2X monopole when mounted on the four glass materials. When the antenna was mounted on clear glass, it had an omni-directional radiation pattern, while the wire-reinforced glass and the vehicle's glass roof showed deep nulls in the radiation pattern, especially at ϴ=90° and 96°. The antenna showed an omni-directional pattern for the low-E glass case but with a gain less than the clear glass antenna mounting. The antenna LAG shown in Figure 4.14 proves that when the antenna is mounted on clear glass, it performs well, like when mounted on metal. The antenna mounted on wire-reinforced glass and glass roof exhibited the worst LAG performance due to the nulls in their radiation patterns.

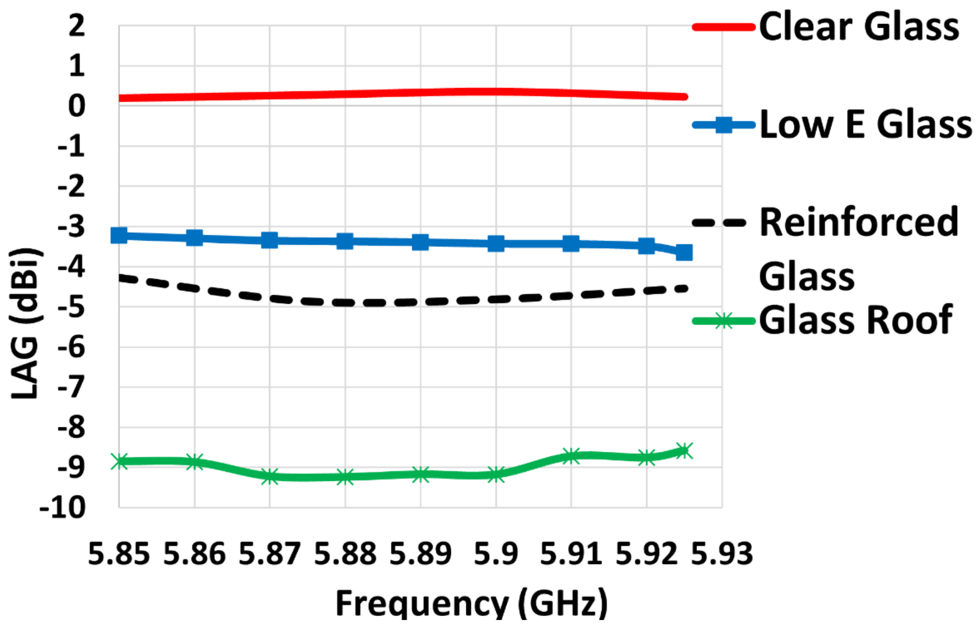

Figure 4.14 C-V2X monopole antenna LAG on four different mounting glass types.

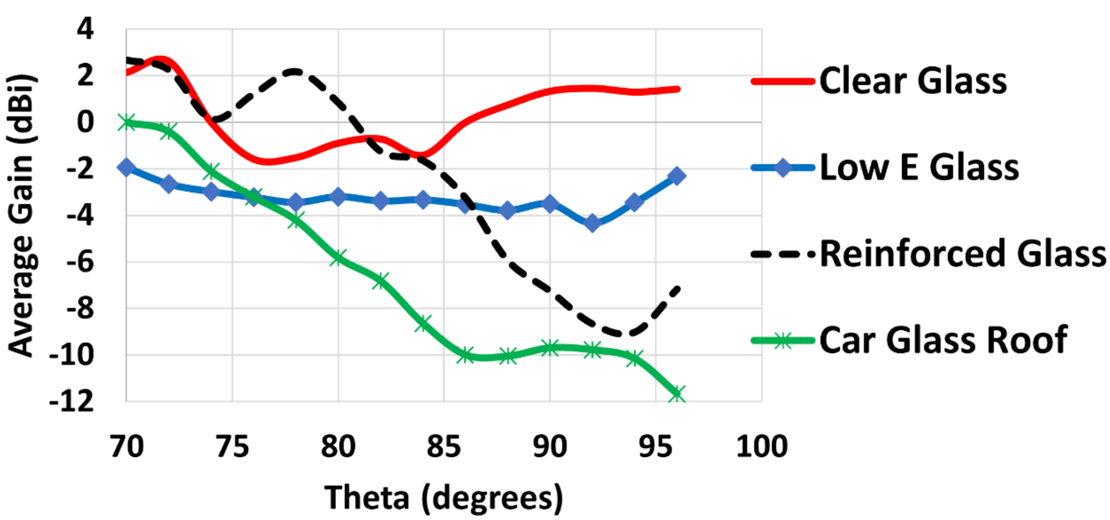

Figure 4.15 C-V2X monopole antenna average gain vs. elevation angles on four different mounting glass types.

Figure 4.15 shows the average gain over elevation angles for the C-V2X monopole antenna mounted on the four glass materials. For the antenna mounted on clear glass and low-E glass, the gain for elevation angles above the horizon (ϴ<90°) and below the horizon have comparable values, while the wire-reinforced glass and the glass-roof showed better gain values in the above-horizon angles compared to the below horizon angles.

These measurements conclude that the glass material is not the reason for the C-V2X monopole antenna performance degradation since the clear glass shows good performance. However, the antenna, mounted on wire-reinforced glass, shows a trend similar to that of the mounted glass roof, indicating that there may be some metallic coating or metallic particles in the construction of the vehicle's glass roof.

4.4 C-V2X Monopole Antenna Simulation on Full Glass Roof

The objective of this section was to get simulation results that matched the measurements for the C-V2X monopole on a glass roof. The antenna measurements on the four glass materials showed the possibility of a metal layer in the glass roof sample, so the best assumption was that there is a low-E coating underneath the glass roof to protect the vehicle interior from heat from the sun. The glass roof CAD files contained opaque areas at the edges of the glass roof while the middle of the glass roof sample was transparent, so we assumed the low E coating layer was in the opaque area at the edges while the transparent area was just pure glass. The low-E coating is a thin transparent coating that is put on the glass to prevent heat and allow the passage of the visible light. One of the low-E coating simplest layer stacks is as follows: Glass-SnO_2(40nm)-Silver(10nm)-SnO_2(40nm) [38,39]. The Tin-Oxide (SnO_2) layer is a high refractive layer which has a dielectric constant of 24 and conductivity of 2 S/m [40,41]. Figure 4.16 shows the layer stack used for the simulation. The antenna is mounted on the glass layer, and then the low E coating is underneath the glass, with each layer having a thickness of

1μm to avoid meshing errors during the simulation when lower thickness values were used.

Figure 4.17 compares the measured and simulated radiation pattern for the C-V2X monopole when mounted on the full glass roof sample. A good agreement is achieved between the simulation and measured radiation pattern, as the simulated radiation pattern shows deep nulls with slight differences from the measurements. For ϴ=96°, the simulated radiation pattern had more reflections in the front direction compared to the measurements. The LAG also agreed well with values of -10 dBi and -9 dBi, for the simulations and measurements, respectively as shown in Figure 4.18. Figure 4.19 shows the simulated and measured average gain over elevation angles for the C-V2X monopole mounted on the glass roof sample. For the elevation angles above the horizon (ϴ<90°), a good agreement was achieved between measurements and simulation. However, for the below horizon elevation angles, a difference of more than 1.5dBi is observed as expected due to the more reflections as shown in the simulated radiation pattern.

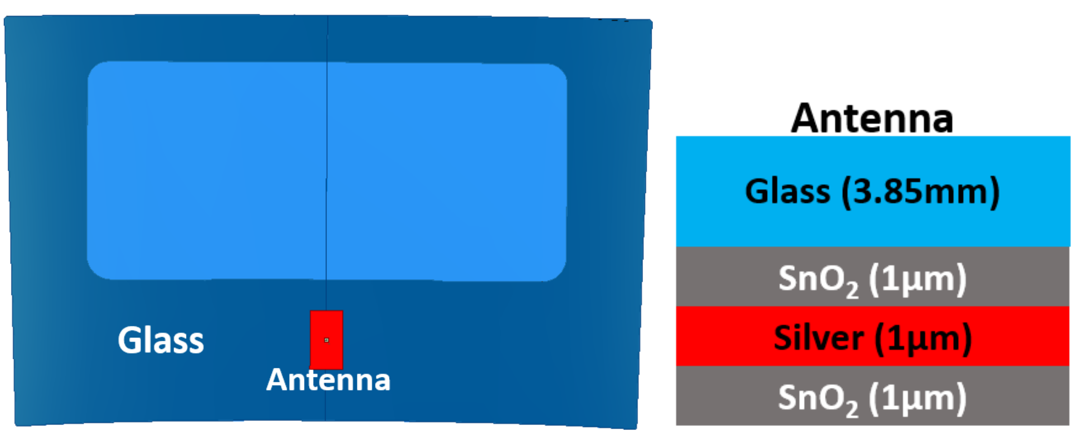

(a) Simulation Setup. (b) Glass Roof Simulation Stack up

Figure 4.16 C-V2X monopole simulation on full glass roof (a) Simulation Setup. (b) Glass Roof Simulation Stack up.

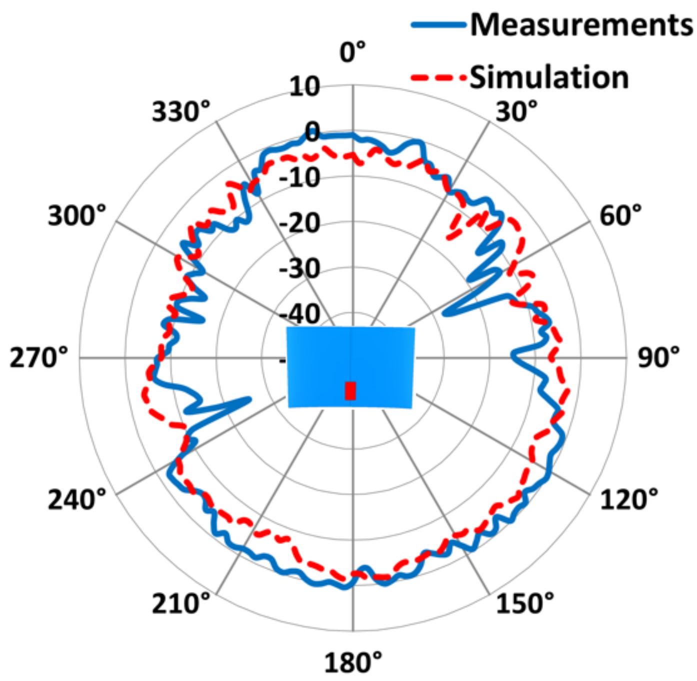

(a) Theta=80°

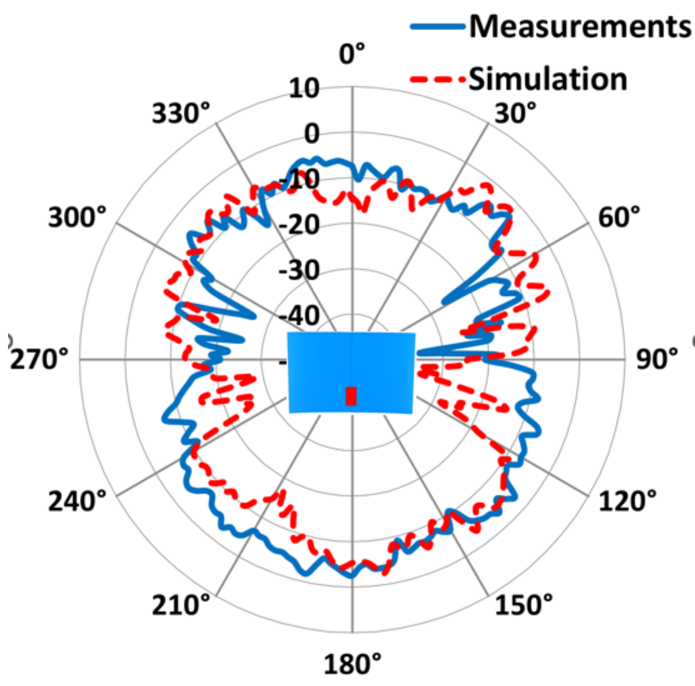

(b) Theta=90°

Figure 4.17 C-V2X monopole antenna measured and simulated radiation pattern on a full glass roof. (a) Theta=80°. (b) Theta=90°. (c) Theta=96°.

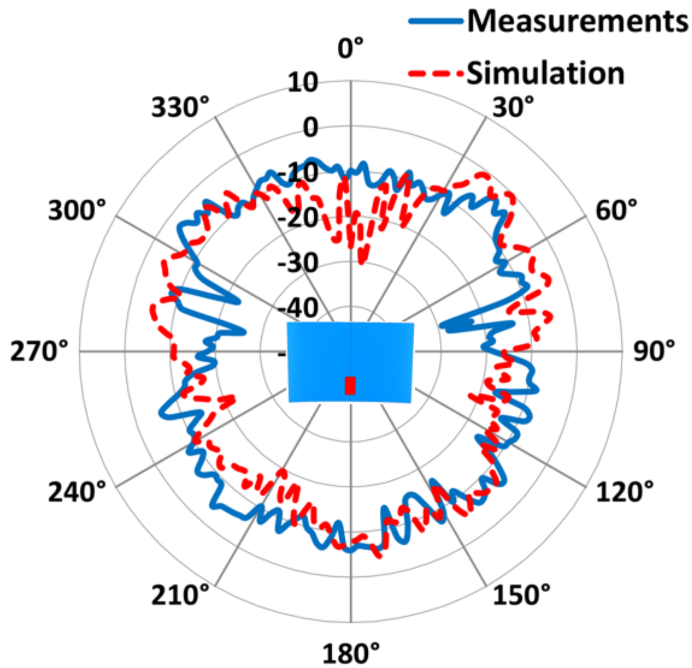

(c) Theta=96°

Figure 4.17 Continued.

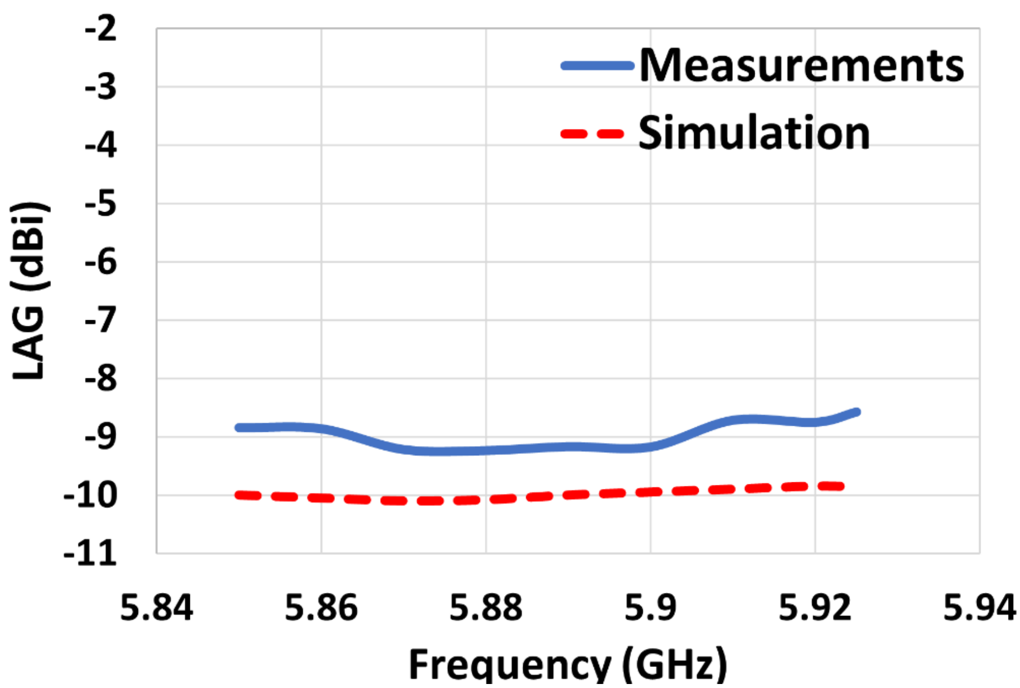

Figure 4.18 C-V2X monopole antenna LAG when mounted on a glass roof measured and simulated.

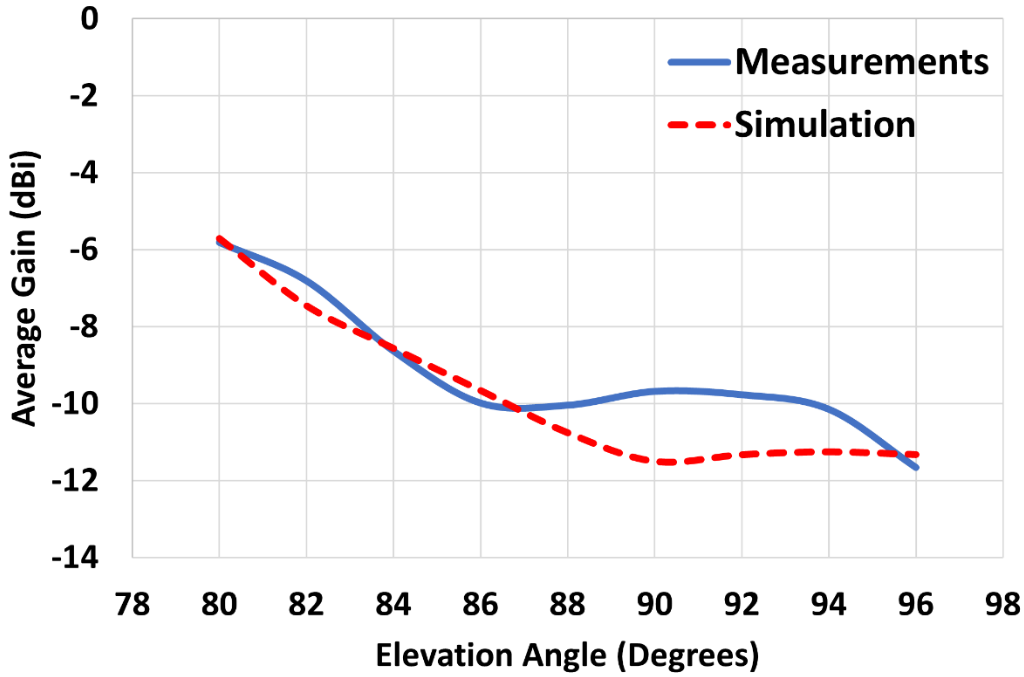

Figure 4.19 C-V2X monopole antenna mounted on a glass roof measured and simulated average gain vs. elevation angles.

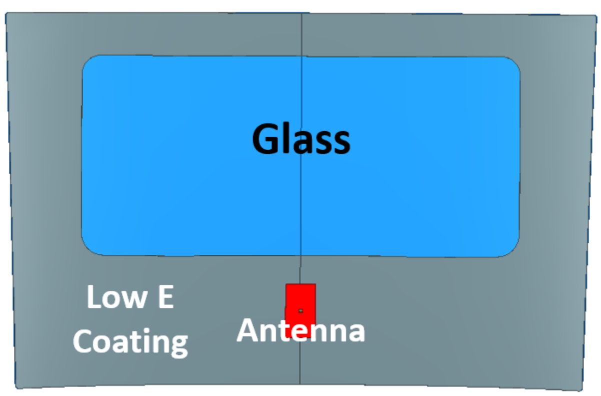

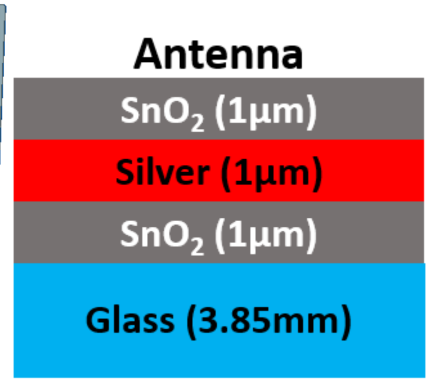

(a) Simulation Setup. (b) Glass Roof Simulation Stack up

Figure 4.20 C-V2X monopole simulation on glass roof with the low E coating on the top (a) Simulation Setup. (b) Glass Roof Simulation Stack up.

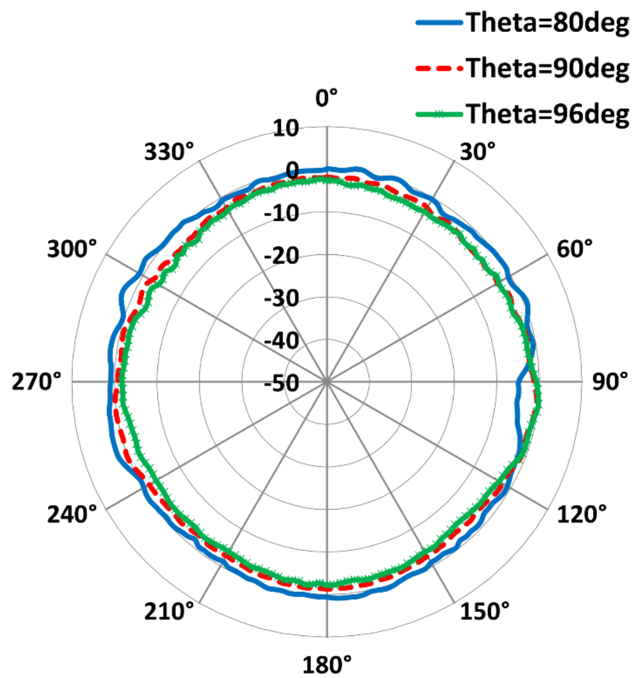

Figure 4.21 C-V2X monopole simulated radiation pattern with the low E coating on the top side of the glass roof for ϴ=80, 90 and 96° at 5.9GHz.

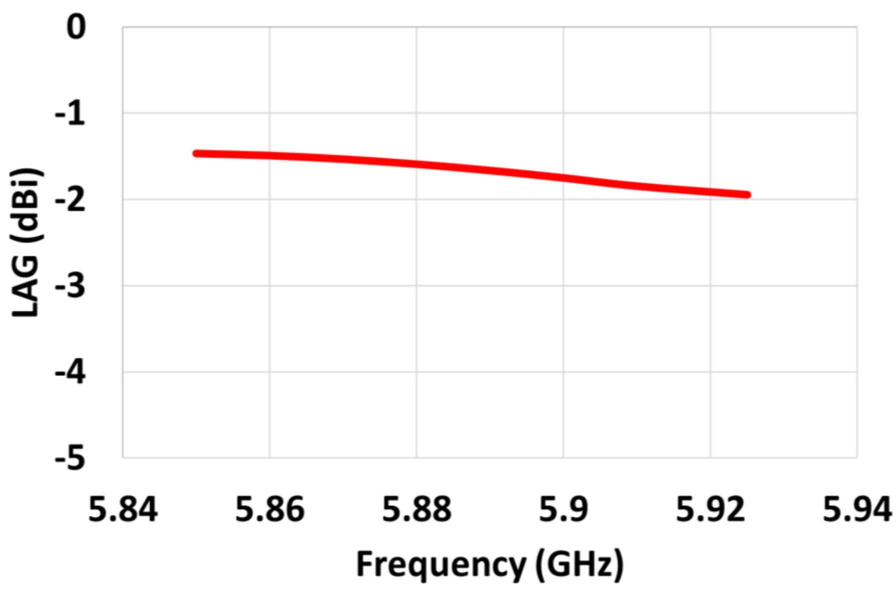

Figure 4.22 C-V2X monopole simulated LAG with the low E coating on the top side of the glass roof.

From the simulation results, the main reason for the C-V2X antenna performance degradation on the glass roof sample is that the C-V2X electromagnetic wave propagates through layers with different dielectric constants, which causes the wave to be reflected and scattered. The reflections that appeared in the measured radiation pattern can prove this analysis. To reduce the wave reflections, the low-E coating can be installed on the upper side of the glass to be between the antenna and the glass layer, as shown in Figure 4.20. An HFSS simulation is performed for the C-V2X antenna when mounted on a glass roof with the low-E coating on the upper side of the glass. Figure 4.21 shows the C-V2X monopole simulated radiation pattern with the low-E coating on the top side of the glass roof. The antenna had good omni-directionality in its radiation pattern at ϴ=80, 90 and 96° without any nulls. Also, the LAG shown in Figure 4.22 was around -1.5 dBi, which is 8 dB better than when the low-E coating on the bottom side. This finding, moving the low-E coating to the top layer of the glass, is crucial for antenna performance improvement on a glass roof resulting in comparable performance when the antenna was mounted on a metallic roof.

4.5 Conclusions

The performance degradation of the C-V2X monopole antenna when mounted on a vehicle's full glass roof is analyzed through a series of measurements and simulations. The analysis showed that the performance degradation is caused by the low-E coating layer underneath the glass in the opaque area at the edges of the glass roof, which caused reflections for the C-V2X electromagnetic waves due to the wave propagation through layers with different dielectric constants. The simulation shows that if the low-E coating is moved from underneath the glass to the top of the glass, the antenna performance will improve significantly.

CHAPTER FIVE

CONCLUSIONS AND FUTURE WORK

5.1 Conclusions

The limited size of the automotive roof-top shark-fin with the increasing number of antennas shows the need for designing multi-band antennas which covers multiple applications and reduce the number of antennas needed. In the first part of this dissertation, a compact monopole antenna is designed to cover multi frequency bands for the automotive industry. The multi-band antenna covers 5G sub-6GHz, LTE, GNSS higher frequency band, and V2X. The proposed antenna is a three-dimensional monopole antenna with two branches to cover the enlarged bandwidth required which starts from 617MHz to 5925MHz. The antenna is simulated, optimized and then a prototype is fabricated and measured on one-meter ground plane and on a vehicle roof. The antenna measurements are expressed in terms of VSWR, radiation pattern, LAG, and efficiency in which the presented antenna showed good results that met the performance requirements. The proposed antenna has measured efficiency of 50-90% in the operating frequency and LAG of -2.2 to 3 dBi across the entire frequency band. A good agreement is achieved between the simulated and measured results. The antenna is optimized to enhance the GNSS performance and the active RHCP LAG is measured which was more than 20 dBi in most of elevation angles using normal 28 dB automotive GNSS LNA.

In the second part of the dissertation, the C-V2X antenna performance degradation when mounted on vehicle full glass roof is investigated. A quarter wave-length C-V2X monopole antenna is used in this investigation. Measurement of the monopole antenna when mounted on vehicle's glass roof shows a performance degradation in LAG of 8 dB compared to when the monopole antenna is mounted on 1m metallic ground plane. The C-V2X monopole antenna is then measured when mounted on four materials, tempered glass, low E glass, wire reinforced glass and vehicle glass roof. When the C-V2X antenna is mounted on tempered glass, the antenna has omni-directional radiation pattern with good LAG. However, when the antenna is mounted on wire reinforced glass and on the car glass roof, deep nulls appeared in the side directions of the radiation pattern with low LAG. This measurements campaign indicates that the C-V2X performance degradation on vehicle's glass roof is not caused by the pure glass and the second finding is that there is some metallic coating or metal particles in the glass roof sample which led to the assumption of the low E coating underneath the glass. The C-V2X monopole antenna is then simulated when mounted on the glass roof sample with the low E coating layer in the opaque area at the edges while the transparent area was just pure glass. An acceptable agreement is achieved between simulation and measurements for the radiation pattern and LAG. The simulation shows that if the low-E coating is moved from underneath the glass to the top, the antenna performance will improve significantly.

5.2 Future Work

Suggestions for the future work include:

- Enhancing the multi-band folded monopole antenna performance in the GNSS frequency band and increase the RHCP gain at zenith.
- Using the multi-band folded monopole antenna to build MIMO system to increase the capacity and throughput of the system.

- Investigating different vehicle's glass roof structures from different automakers and study their effects on the C-V2X antennas then propose solutions to avoid antenna performance degradation when mounted on glass roof.
- Exploring using hidden C-V2X antennas, the antennas can be distributed inside the vehicle to provide the C-V2X omni-directional coverage required. Hidden and distributed C-V2X antennas can be useful to avoid antenna performance degradation due to the glass roof and to meet vehicle's aesthetic requirements.

REFERENCES

[1] S. Rao, N. Llombart, D. Zamberlan and M. Pannozzo, "Potential implications and road mapping of satellite bidirectional s-band antennas in the automotive market [antenna applications corner]," in IEEE Antennas and Propagation Magazine, vol. 56, no. 2, pp. 240-250, April 2014, doi: 10.1109/MAP.2014.6837094.

[2] N. Koch, "Antennas for Automobiles", in New Advances in Vehicular Technology and Automotive Engineering. London, United Kingdom: IntechOpen, 2012.

[3] Balanis, Constantine A. Antenna theory: analysis and design. John wiley & sons, 2016.

[4] Liu, L., S. W. Cheung, Y. F. Weng, T. I. Yuk, and M. Matin. "Cable effects on measuring small planar UWB monopole antennas." In Ultra Wideband—Current Status and Future Trends. London, UK: InTech, 2012.

[5] J. A. Ray and S. R. B. Chaudhuri, "A review of PIFA technology," 2011 Indian Antenna Week (IAW), Kolkata, India, 2011, pp. 1-4, doi: 10.1109/IndianAW.2011.6264946.

[6] https://www.antenna-theory.com/antennas/patches/pifa.php

[7] Lawal AB. Fundamentals of Satellite Navigation Systems: How to Design GPS/GNSS Receivers Book 1: The Principles, Applications & Markets. AB Lawal; 2018 Dec 3.

[8] Ahmad S. Ibrahim, Ahmad M. Yacoub, and Daniel N. Aloi. "A 3-Dimensional Multiband Antenna for Vehicular 5G Sub-6 GHz/GNSS/V2X Applications." International Journal of Antennas and Propagation 2022.

[9] G. Artner, W. Kotterman, G. Del Galdo and M. A. Hein, "Automotive Antenna Roof for Cooperative Connected Driving," in IEEE Access, vol. 7, pp. 20083-20090, 2019, doi: 10.1109/ACCESS.2019.2897219.

[10] E. Ghafari, A. Fuchs, D. Eblenkamp and D. N. Aloi, "A vehicular rooftop, shark-fin, multiband antenna for the GPS/LTE/cellular/DSRC systems," 2014 IEEE-APS Topical Conference on Antennas and Propagation in Wireless Communications (APWC), 2014, pp. 237-240, doi: 10.1109/APWC.2014.6905546.

[11] M. B. Diez, W. Pascher and S. Lindenmeier, "Electromagnetic characterization of automotive sunroofs for car-to-X applications," 2016 46th European Microwave Conference (EuMC), 2016, pp. 1323-1326, doi: 10.1109/EuMC.2016.7824595.

[12] D. Preradovic and D. N. Aloi, “Cross polarized 2x2 LTE MIMO system for automotive shark fin application,” The Applied Computational Electromagnetics Society (ACES), vol. 35, no. 10, pp. 1207-1216, Oct. 2020.

[13] S. Arianos, G. Dassano, F. Vipiana and M. Orefice, "Design of Multi-Frequency Compact Antennas for Automotive Communications," in IEEE Transactions on Antennas and Propagation, vol. 60, no. 12, pp. 5604-5612, Dec. 2012, doi: 10.1109/TAP.2012.2213052.

[14] Y. Liu, Z. Ai, G. Liu and Y. Jia, "An Integrated Shark-Fin Antenna for MIMO-LTE, FM, and GPS Applications," in IEEE Antennas and Wireless Propagation Letters, vol. 18, no. 8, pp. 1666-1670, Aug. 2019, doi: 10.1109/LAWP.2019.2927019.

[15] V. Franchina et al., "A compact 3D antenna for automotive LTE MIMO applications," 2017 IEEE-APS Topical Conference on Antennas and Propagation in Wireless Communications (APWC), 2017, pp. 326-329, doi: 10.1109/APWC.2017.8062317.

[16] A. Friedrich, B. Geck, O. Klemp and H. Kellermann, "On the design of a 3D LTE antenna for automotive applications based on MID technology," 2013 European Microwave Conference, 2013, pp. 640-643, doi: 10.23919/EuMC.2013.6686737.

[17] I. Goncharova and S. Lindenmeier, "A high efficient automotive roof-antenna concept for LTE, DAB-L, GNSS and SDARS with low mutual coupling," 2015 9th European Conference on Antennas and Propagation (EuCAP), 2015, pp. 1-5.

[18] I. Goncharova and S. Lindenmeier, "A high-efficient 3-D Nefer-antenna for LTE communication on a car," The 8th European Conference on Antennas and Propagation (EuCAP 2014), 2014, pp. 3273-3277, doi: 10.1109/EuCAP.2014.6902527.

[19] M. O. Khalifa, A. M. Yacoub and D. N. Aloi, "A Multiwideband Compact Antenna Design for Vehicular Sub-6 GHz 5G Wireless Systems," in IEEE Transactions on Antennas and Propagation, vol. 69, no. 12, pp. 8136-8142, Dec. 2021, doi: 10.1109/TAP.2021.3083770.

[20] A. M. Yacoub, M. O. Khalifa and D. N. Aloi, "Design of Multi-Wideband Automotive Cell Antenna for LTE and 5G Applications," 2021 15th European Conference on Antennas and Propagation (EuCAP), 2021.

[21] B. Sanz-Izquierdo, S. Jun, J. Heirons and N. Acharya, "Inkjet printed and folded LTE antenna for vehicular application," 2016 46th European Microwave Conference (EuMC), 2016, pp. 88-91, doi: 10.1109/EuMC.2016.7824284.

[22] Yong Cheng, Jing Lu, Can Wang, "Design of a Multiple Band Vehicle-Mounted Antenna", International Journal of Antennas and Propagation, vol. 2019, Article ID 6098014, 11 pages, 2019.

[23] Ahmad Yacoub, Mohamed Khalifa, and Daniel N. Aloi, "Wide Bandwidth Low Profile PIFA Antenna for Vehicular Sub-6 GHz 5G and V2X Wireless Systems," Progress In Electromagnetics Research C, Vol. 109, 257-273, 2021.

[24] Y. Dong, J. Choi and T. Itoh, "Vivaldi Antenna With Pattern Diversity for 0.7 to 2.7 GHz Cellular Band Applications," in IEEE Antennas and Wireless Propagation Letters, vol. 17, no. 2, pp. 247-250, Feb. 2018, doi: 10.1109/LAWP.2017.2783323.

[25] A. Michel, P. Nepa, M. Gallo, I. Moro, A. P. Filisan and D. Zamberlan, "Printed Wideband Antenna for LTE-Band Automotive Applications," in IEEE Antennas and Wireless Propagation Letters, vol. 16, pp. 1245-1248, 2017, doi: 10.1109/LAWP.2016.2629619.

[26] D. V. Navarro-Méndez et al., "Compact Wideband Vivaldi Monopole for LTE Mobile Communications," in IEEE Antennas and Wireless Propagation Letters, vol. 14, pp. 1068-1071, 2015, doi: 10.1109/LAWP.2015.2389956.

[27] S. Hastürkoğlu and S. Lindenmeier, "A wideband automotive antenna for actual and future mobile communication 5G/LTE/WLAN with low profile," 2017 11th European Conference on Antennas and Propagation (EUCAP), 2017, pp. 602-605, doi: 10.23919/EuCAP.2017.7928669.

[28] O. -Y. Kwon, R. Song and B. -S. Kim, "A Fully Integrated Shark-Fin Antenna for MIMO-LTE, GPS, WLAN, and WAVE Applications," in IEEE Antennas and Wireless Propagation Letters, vol. 17, no. 4, pp. 600-603, April 2018, doi: 10.1109/LAWP.2018.2805681.

[29] J. D. Doherty, I. Shoaib, X. Chen and C. Parini, "Study and design of an integrated GPS and cellular antenna," 2013 Loughborough Antennas & Propagation Conference (LAPC), 2013, pp. 587-590, doi: 10.1109/LAPC.2013.6711968

[30] P. Mousavi, "Multiband Multi-polarization Integrated Monopole Slots Antenna for Vehicular Telematics Applications," in IEEE Transactions on Antennas and Propagation, vol. 59, no. 8, pp. 3123-3127, Aug. 2011, doi: 10.1109/TAP.2011.2158949.

[31] S. Wu, C. Kang, K. Chen and J. Tarng, "A Multiband Quasi-Yagi Type Antenna," in IEEE Transactions on Antennas and Propagation, vol. 58, no. 2, pp. 593-596, Feb. 2010, doi: 10.1109/TAP.2010.2041522.

[32] Y. Wang, Y. Li and Q. Zhu, "A compact tri-band antenna for GPS and GSM applications," 2017 Sixth Asia-Pacific Conference on Antennas and Propagation (APCAP), 2017, pp. 1-3, doi: 10.1109/APCAP.2017.8420367.

[33] M. B. Diez, P. Plitt, W. Pascher and S. Lindenmeier, "Antenna placement and wave propagation for Car-to-Car communication," 2015 European Microwave Conference (EuMC), 2015, pp. 207-210, doi: 10.1109/EuMC.2015.7345736.

[34] M. B. Diez, W. Pascher and S. Lindenmeier, "Electromagnetic characterization of automotive sunroofs for car-to-X applications," 2016 46th European Microwave Conference (EuMC), 2016, pp. 1323-1326, doi: 10.1109/EuMC.2016.7824595.

[35] M. Niebisch, T. Deinlein, D. Pfaller, R. German and A. Djanatliev, "Impact of the Communication Direction on the Reliability of Vehicle-to-Everything (V2X) Communications," 2020 IEEE Vehicular Networking Conference (VNC), New York, NY, USA, 2020, pp. 1-7, doi: 10.1109/VNC51378.2020.9318416.

[36] A. Kwoczek, Z. Raida, J. Láčík, M. Pokorny, J. Puskelý and P. Vágner, "Influence of car panorama glass roofs on Car2Car communication (poster)," 2011 IEEE Vehicular Networking Conference (VNC), Amsterdam, Netherlands, 2011, pp. 246-251, doi: 10.1109/VNC.2011.6117107.

[37] Sayidmarie, K. and L. Yahya, "Modeling of dual-band crescent-shape monopole antenna for WLAN applications," International Journal of Electromagnetics and Applications, Vol. 4, 31–39, doi:10.5923/j.ijea.20140402.01, 2014.

[38] Bräuer G. "Large area glass coating, " Surface and Coatings Technology, 112, 1999, pp. 358-365.

[39] Jelle, Bjørn Petter, Simen Edsjø Kalnæs, and Tao Gao. "Low-emissivity materials for building applications: A state-of-the-art review and future research perspectives." Energy and Buildings 96 (2015): 329-356.

[40] Hallil, Hamida, Philippe Menini, and Hervé Aubert. "Novel microwave gas sensor using dielectric resonator with SnO2 sensitive layer." Procedia Chemistry 1, no. 1 (2009): 935-938.

[41] Zhou, Min, et al. "Electrospun SnO2 submicron fibers for broadband microwave absorption." Journal of Physics D: Applied Physics 48.49 (2015): 495303.